



Long-term variation of cloud droplet number concentrations from space-based Lidar



Jiming Li^a, Bida Jian^a, Jianping Huang^{a,*}, Yongxiang Hu^b, Chuanfeng Zhao^{c,e}, Kazuaki Kawamoto^d, Shujie Liao^a, Min Wu^a

^a Key Laboratory for Semi-Arid Climate Change of the Ministry of Education, College of Atmospheric Sciences, Lanzhou University, Lanzhou, China

^b Climate Science Branch, NASA Langley Research Center, Hampton, VA, USA

^c State Key Laboratory of Earth Surface Processes and Resource Ecology, Beijing Normal University, Beijing, China

^d Graduate School of Fisheries and Environmental Sciences, Nagasaki University, Nagasaki, Japan

^e College of Global Change and Earth System Science, Beijing Normal University, Beijing, China

ARTICLE INFO

Keywords:

Cloud droplet number concentration
Aerosol mass concentration
CALIPSO
MODIS
MERRA2

ABSTRACT

This study presents a new 10 year of liquid water cloud droplet number concentration (N_d) climatology, and analyzes its long-term variation on both regional and global scales based on accurate depolarization ratio measurement from CALIPSO and 3.7 μm cloud effective radius retrieval from MODIS. Compared with the widely used passive retrieval method (e.g., MODIS retrieval), which considers N_d as function of cloud optical depth, geometry thickness and effective radius, retrieval method of the new N_d dataset has a weak dependence upon the cloud adiabatic assumption and eliminates the possible bias caused by multilayer clouds. Statistical results show that the annual cycle and long-term variability of N_d retrieved by CALIPSO agree reasonably well with those obtained from MODIS retrieval method, especially over the stratocumulus regions (correlation coefficient > 0.9). Multiple regression models and contribution calculation verify that the variability of sulfate mass concentration dominates the long-term variation of N_d over most regions, even though the contribution factors and rates vary with different regions, temperatures and methods. In addition, our study also indicates that the impact of BC and OC on N_d should not be ignored, especially for supercooled water clouds over those important biomass burning regions. These results demonstrate the temperature-dependent N_d climatology derived from CALIOP has potential to be beneficial to climate research and reduce the uncertainties in estimates of the aerosol indirect effect in the model simulations.

1. Introduction

Liquid water clouds (e.g., stratiform boundary layer) play a key role in modulating the earth's climate by changing their radiative (e.g., shortwave reflection and infrared emission) (Brenquier et al., 2000; Garrett and Zhao, 2006; Klein and Hartmann, 1993) and precipitation properties (Lohmann and Feichter, 2005). Their formations and variations are closely controlled by the relevant dynamical (Klein and Hartmann, 1993; Myers and Norris, 2016; Seethala et al., 2015; Wood, 2012) and microphysical processes (McCoy et al., 2015, 2017a; Quaas et al., 2009). Higher atmospheric aerosol loading from anthropogenic activities (e.g., rapid industrialization) and natural processes (e.g., volcanic eruptions) may influence cloud properties in various ways. Among many others, the most direct effect of aerosols on clouds is that aerosols serve as cloud condensation nuclei (CCN), increasing the cloud

droplet number concentration (N_d) and decreasing the effective radius, thereby enhancing the reflectivity of solar radiation by clouds for a given cloud liquid water content (i.e., “the first aerosol indirect effect” or “Twomey effect”) (Twomey, 1977). While any disturbance of N_d caused by increased aerosol concentrations may significantly influence cloud albedo and possibly regionally counteract greenhouse warming, the strength of the first indirect aerosol effect is still a highly uncertain component of the overall global radiative forcing estimation made using global climate models (Ramaswamy et al., 2001). One of the prominent problems is that models fail to capture all the key controls of N_d ; thus, they usually employ distinctly different values of N_d and its lower bounds, such that they exhibit a wide range of uncertainty in the simulated magnitudes of the first indirect effect (Lohmann et al., 2007; Quaas et al., 2008). A previous study has shown that the simulated indirect aerosol effect can be reduced by up to 80% when models

* Corresponding author at: Key Laboratory for Semi-Arid Climate Change of the Ministry of Education, College of Atmospheric Sciences, Lanzhou University, Lanzhou, Gansu 730000, China.

E-mail address: hjp@lzu.edu.cn (J. Huang).

<https://doi.org/10.1016/j.rse.2018.05.011>

Received 31 January 2018; Received in revised form 4 May 2018; Accepted 7 May 2018

0034-4257/ © 2018 Elsevier Inc. All rights reserved.

constrain the lower bounds of N_d without regard for the simulated concentrations of activated aerosols (Hoose et al., 2009).

In recent decades, many efforts have been made to decrease the uncertainties of the first indirect effects of the model simulations based on satellite observations, in situ measurements and field campaigns (e.g., Chubb et al., 2016; Huang et al., 2014; Garrett et al., 2004; Lohmann et al., 2000, 2007; Schmidt et al., 2013, 2014; Wang et al., 2010). Ground-based lidar observations and airborne measurements may provide more accurate N_d values, but only limited temporal and spatial coverages are possible (Allen et al., 2011; Donovan et al., 2015; Lu et al., 2007; Schmidt et al., 2015). Thus, the results from in situ observational measurements are commonly used to validate and evaluate satellite-derived N_d (e.g., Ahmad et al., 2013; Painemal and Zuidema, 2011). Until now, the satellite retrieval of N_d has been challenging, and different methods have been presented to derive the climatology of N_d or its precursor (that is, cloud condensation nuclei) (e.g., Bennartz, 2007; Bennartz and Rausch, 2017; Brenguier et al., 2000; Han et al., 1998; Hu et al., 2007a; Rosenfeld et al., 2012, 2016; Schuller et al., 2005). The one method that has been widely used is based on the assumption of an “adiabatic cloud model” and considers the cloud droplet number concentration as a function of cloud optical depth (τ), cloud geometry thickness (H) and effective radius (r_e) at the cloud top (Bennartz, 2007; Brenguier et al., 2000; Schuller et al., 2005). However, most of the clouds in the atmosphere are not strictly adiabatic. Precipitation processes or other factors (e.g., cloud top entrainment) may lead to the clouds being under the sub-adiabatic condition (Wood, 2012; Wood et al., 2012). In contrast to the passive method, Hu et al. (2007a) developed a novel approach to evaluate N_d by combining the lidar depolarization ratio measurements from CALIPSO and the cloud effective radius from MODIS. This method has a weak dependence on the adiabatic assumption and is independent of cloud type. By using one year of data from CALIPSO and MODIS, Zeng et al. (2014) found similar geographical distributions and seasonal variations of N_d between the above two methods. As a result, the advantage of CALIPSO is that it allows us to build a new N_d climatology and further analyze the consistency of the long-term variations between the two N_d datasets.

Such a long-term N_d dataset will be beneficial to determine the factors that contribute to this temporal variability of N_d at the global and regional scales. Many observations and model simulations have verified that increased aerosol concentrations may result in increased N_d (e.g., Bennartz, 2007; Bennartz et al., 2011; Snider et al., 2003). In addition to aerosol concentrations, N_d is also associated with the aerosol size distribution, chemical composition and meteorological conditions (e.g., updraft velocity at cloud base) (Chubb et al., 2016; Reutter et al., 2009; Wood et al., 2012). Reutter et al. (2009) used a cloud parcel model to investigate the dependence of N_d on the aerosol number concentrations and updraft velocities, and found that the sensitivity of N_d to aerosols and velocity varies with region. Karydis et al. (2012) tested the adjoint sensitivity of global N_d values to aerosol and dynamic parameters. Their simulation showed that N_d is more sensitive to updraft velocities and water uptake coefficients (aerosol number concentration and hygroscopicity) over polluted (pristine) areas. Over the southern oceans, McCoy et al. (2015) analyzed the correlations between N_d and aerosols, and noted that natural aerosols affect the spatiotemporal variability of N_d and may explain the seasonal and spatial patterns of the Southern Ocean cloud albedo, which is consistent with the results of the study by Karydis et al. (2012). However, a recent model simulation demonstrated that the updraft velocity is the primary driver of N_d variability for 45.5% of the grid, and the sensitivity of the temporal variability of N_d to the velocity cannot be neglected over the southern oceans (Sullivan et al., 2016). Thus, to reconcile such an inconsistency between model simulations, we perform an adjoint sensitivity analysis of N_d to aerosol type and vertical velocity by using two satellite-observed N_d datasets derived from CALIPSO and MODIS, the aerosol properties from the Modern-Era Retrospective Analysis for Research and Applications Version 2 (MERRA2) and the updraft velocities

from the ERA-interim and MERRA2 datasets. Based on this investigation, we attempt to focus on two key points: (1) What factors drive the temporal variability of N_d at regional and global scales? (2) Which one is the dominant factor? Although some statistical results agree reasonably well with previous studies, new insights are also presented.

This paper is organized as follows. A brief introduction to all the datasets and retrieval methods used in this study is given in Section 2. Section 3.1 prescribes the comparisons of the geographical, annual and long-term variations of the N_d between the two retrieval methods. Further analyses of the contributions of the aerosols and vertical velocities to the long-term variabilities of regional N_d are provided in Section 3.2. Finally, the conclusions are presented in Section 4.

2. Datasets and methodology

In this study, 10 years (2007–2016) of data from the Aqua-MODIS collection 6 level-2 cloud product (MYD06), the CALIPSO Lidar level-2 cloud layer products, and the daily 3-hour aerosol product from the MERRA2 reanalysis were collected. Then, these datasets are used to retrieve the liquid water cloud droplet number concentrations during the daytime and to discuss the contributions from different factors on its temporal variability.

2.1. Satellite products and reanalysis dataset

The effective cloud radius of 3.7 μm (r_e), cloud optical thickness (τ), cloud multi-layer flag (CMLF) with a spatial resolution at the nadir of 1 \times 1 km, and cloud fraction (CF) with a spatial resolution at 5 \times 5 km from the Aqua-MODIS level-2 collection 6 cloud products (MYD06) (Platnick et al., 2015, 2017) during the daytime were used in our study. Compared with the MODIS collection of 5 cloud products, several improvements have been made (Rausch et al., 2017), such as significant improvements in the forward radiative transfer models.

The collocated CALIPSO level-2 1 km (v4.10) cloud layer product provides essential cloud thermodynamic phases (e.g., water, randomly oriented ice, horizontally oriented ice or unknown phase) at the cloud top, the cloud top and base height (temperature and pressure) information, the layer-integrated volume depolarization ratio and the number of cloud layers in a given Lidar profile (Hu et al., 2009). Compared with the earlier CALIOP version 3 products, there have been several substantial improvements made to increase the retrieval accuracies of the parameters needed to determine the N_d from Lidar (e.g., improved cloud subtypes and ice-water phase determination).

In addition, the Modern-Era Retrospective Analysis for Research and Applications Version 2 (MERRA2) combines measurements of the atmospheric states and remotely sensed aerosol optical depths to provide the aerosol reanalysis (Buchard et al., 2015; Molod et al., 2015), which has been evaluated by CALIOP measurement in recent studies (Buchard et al., 2017; Nowottnick et al., 2015; Li et al., 2016). Here, the daily 3-hour aerosol and meteorological products from the MERRA2 reanalysis, which have gridded resolutions of 0.5° \times 0.625°, are also used to provide the related information of the updraft velocity (w) and mass concentration of different aerosol species at several pressure levels. The MERRA2 product can supply the mass mixing ratios of eight aerosol types, including black carbon (BC), dimethyl sulfide (DMS), dust (DU), methane sulfonic acid (MSA), organic carbon (OC), sulfate aerosol (SO₄), sulfur dioxide (SO₂) and sea salt (SS). Some studies have addressed the effects of MSA, OC, BC, sulfate and SS aerosols as cloud condensation nuclei (CCN) (Ayers and Gras, 1991; Lammel and Novakov, 1995; O'Dowd et al., 1997; Ruehl et al., 2016; Sun and Ariya, 2006). Following the studies of Sullivan et al. (2016) and McCoy et al. (2017b), this investigation uses only the mass mixing ratios of hydrophilic OC, BC, SO₄, SO₂ and the smallest particles of SS (that is, 0.03–0.1 μm size bin) and dust (that is, 0.1–1 μm size bin) to calculate their mass concentrations at different pressure levels. In addition, the daily 6-hour vertical velocities from the ERA-interim reanalysis

(resolution of $0.5^\circ \times 0.5^\circ$) are also used in our analysis and are collocated to MERRA2 to obtain the best representations of vertical velocities w . The positive vertical velocity in this study implies an updraft.

2.2. Retrieval of N_d based on CALIOP and MODIS measurements

Based on a Monte Carlo simulation, Hu et al. (2007a) provided a robust empirical relationship between the extinction coefficient β , the effective radius r_e and the layer-integrated depolarization ratio δ , that is,

$$\beta = \left(\frac{r_e}{1\mu m}\right)^{1/3} \left[1 + 135\frac{\delta^2}{(1-\delta)^2}\right] \quad (1)$$

For almost all of current remote sensing algorithms, the droplet size distribution of water clouds are assumed as log-normal or gamma size distributions (Zhao et al., 2012). By assuming that the water clouds have a generalized gamma size distribution (Hu and Stamnes, 1993), then the true droplet number concentration N_d can be approximated as:

$$N_d = N_e \frac{(\gamma + 2)^2}{(\gamma + 1)\gamma} \quad (2)$$

where N_e (unit: cm^{-3}) is the effective number concentration of a water cloud with a mono-disperse droplet size distribution and may be expressed as:

$$N_e = \frac{\beta}{2\pi r_e^2} = 1000 \frac{1 + 135\delta^2/(1-\delta)^2}{2\pi (r_e/1\mu m)^{5/3}} \quad (3)$$

where γ is the width of the generalized gamma size distribution and $(\gamma + 2)^2/(\gamma + 1)\gamma$ is the ratio of the effective radius to the volume radius of a liquid droplet. By comparing all available aircraft observations of water clouds, Miles et al. (2000) discussed the appropriateness of the assumptions used in the remote sensing of cloud droplet size distribution parameters. Their work found that the value of γ has a relatively wide range in different observations. For example, the γ has small value (around 3) for the stratocumulus observation in the North sea from Martin et al. (1994), to 15 for stratus observation in the west of Santa Cruz from Ryan et al. (1972), to even more larger values (> 20) for thick nocturnal stratocumulus observation by Slingo et al. (1982). Such wide range of γ in different observations would be linked to the availability of CCN, their size distribution and chemical composition, as well as the meteorological condition. Generally speaking, the mean values of γ are 8.6 for marine clouds and 8.7 for the continental clouds based on the statistical results from Miles et al. (2000). It means that the retrieved droplet number concentration N_d will be $2.1N_e$, $1.36N_e$, $1.2N_e$, and $1.15N_e$ for γ values of 3, 8.6, 15 and 20, respectively. These results indicate that the application of one fixed γ value in all regions should result in some uncertainties in the N_d retrieval. Until now, however, it has remained difficult to derive accurate climatological values of γ for different regions due to very limited observations. For comparing with the MODIS retrieval, we apply a constant value (12.3) of γ for marine and continental clouds, and the corresponding effective variance of the gamma distribution $1/(\gamma + 2)$ is 0.07. This value approaches the value used in MODIS retrieval (Bennartz and Rausch, 2017). In addition to the width of the size distribution, some potential error sources may also affect the retrieval accuracy of N_d , although this method is independent of the adiabatic assumption. For example, Zeng et al. (2014) analyzed the advantages and weaknesses of different retrieval methods of N_d and discussed the impacts of cloud entrainment, drizzling, horizontal heterogeneities and effective radii on the retrieval of N_d . After assuming the value of γ , the true droplet number concentration N_d of a single-layered cloud can be retrieved based on Eqs. (2) and (3) by combining the depolarization ratio measurements from CALIPSO and the effective radii from the MODIS 3.7 μm channel. Here, it is worth noting that the N_d from this method is a numerical concentration at the cloud top layer because of the limited penetration depth of the 3.7 μm solar radiation

and Lidar signal into clouds (Hu et al., 2007a).

2.3. Retrieval of N_d from Aqua-MODIS measurements

The N_d retrieval method based on the MODIS measurements originates from an ‘‘adiabatic cloud model’’ assumption (Bennartz, 2007; Brenguier et al., 2000; Schuller et al., 2005), which assumes that cloud liquid water content increases linearly from the cloud base to the top, and the value of N_d within the cloud remains constant with height. Under this assumption, the N_d is approximately given as:

$$N_d = \frac{\tau^3}{k} [2W]^{-5/2} \left[\frac{3\pi Q}{5}\right]^{-3} \left[\frac{3}{4\pi\rho}\right]^{-2} c_w^{1/2} \quad (4)$$

where τ is the cloud optical depth, $Q \approx 2$ is the scattering efficiency of cloud droplets, ρ is the water density, c_w is the condensation rate, W is cloud liquid water path, and $k = 0.8$ is the ratio between the volume mean radius and the effective radius. The cloud liquid water path may be expressed as: $W = \frac{5\rho r_e}{9} = \frac{1}{3}c_w H^2$, where r_e is the effective radius of the cloud top at 3.7 μm , and H is the cloud thickness. Following the definition from Grabowski (2007), the condensation rate c_w is a function of temperature (here, we use the cloud top temperature from MODIS), pressure (from the CALIOP cloud product) and water vapor saturation pressure (a function of the temperature defined by Lindblom and Nordell (2006)). To date, this method has been widely used for climate model validation and evaluation (Hoese et al., 2008; Wang et al., 2015; Zhang et al., 2012) and for the estimation of the first aerosol indirect effect (McCoy et al., 2015, 2017b). Nevertheless, some weaknesses and error sources related to N_d retrievals were also noted in many studies (e.g., Grosvenor and Wood, 2014; Rosenfeld et al., 2012; Wood et al., 2012; Zhang et al., 2016). Recently, Bennartz and Rausch (2017) improved the accuracies of retrieved N_d values by applying some additional screening criteria and published the latest N_d dataset ($1^\circ \times 1^\circ$ resolution) based on 13 years of Aqua-MODIS measurements. In their study, the uncertainties caused by several potential error sources (e.g., broken clouds and observation geometry) were also assessed and quantified. Generally, accurate retrievals of N_d from satellites are rather complex and suffer from many uncertainties. Cloud entrainment, drizzling, horizontal heterogeneity and observation geometry may all result in some biases in the Lidar-derived and MODIS-derived N_d (Bennartz and Rausch, 2017; Grosvenor and Wood, 2014; Wood et al., 2012). However, additional uncertainty can also be caused by vertical cloud overlaps in the MODIS retrieval method (McCoy et al., 2017b; Sourdeval et al., 2015, 2016). For example, based on the comparison between the MODIS-derived N_d and the long-term measurements of N_d , Ahmad et al. (2013) showed that the number of cloud layers is very important when matching the ground-based measurements to the MODIS retrieval, and the correlation between the retrieved and observed N_d values will be greatly improved when only single-layer clouds exist. In addition, k value, which is determined by the skewness and dispersion of the droplet size distribution, is setted as 0.8 and represents similar width of the generalized gamma size distribution (e.g., γ value) used in CALIPSO method. Bennartz and Rausch (2017) showed that a realistic uncertainty estimate for k between different studies is around 20%.

2.4. Building the gridded climatologies of N_d based on different methods

For the data processing, each Lidar profile of the CALIPSO level-2 1 km cloud layer product is first matched with a MODIS pixel-level observation in both space (e.g., distance < 1 km) and time (e.g., time difference < 90 s) in order to ensure they point to the same clouds. In this study, we focus only on the retrieval of the N_d of a single-layered (that is, ‘‘number of cloud layers’’ set to be 1) liquid cloud due to the passive sensors is difficult to accurately retrieve multilayer cloud properties (e.g., cloud phase, particle size or cloud top temperature)

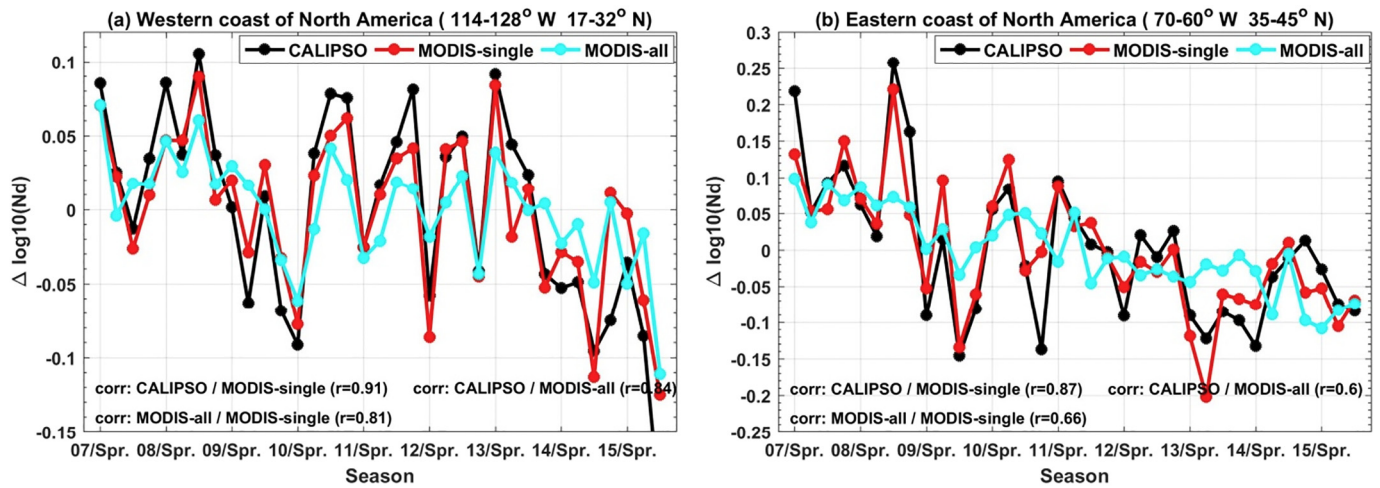


Fig. 1. The comparison of time series of $\Delta \log_{10}(N_d)$ over different regions based on three datasets. Here, CALIPSO and MODIS-single datasets are from our study, and MODIS-all dataset is from the study of [Bennartz and Rausch \(2017\)](#).

([Huang, 2006](#); [Huang et al., 2005, 2006](#); [Minnis et al., 2007](#); [Wang et al., 2016](#)). Passive satellite cloud property retrievals are typically based on the single-layer cloud assumption, and any error from the MODIS retrieval of cloud properties will be propagated to the calculation of N_d . Based on this consideration, this study only considers the single-layer liquid phase clouds with a high confidence by using the cloud phase information of the “feature classification flags” from CALIPSO, and limiting the “cloud layer number” from CALIPSO and “cloud multilayer flag” from MODIS to 1. In the MODIS product, the multilayer cloud detection algorithm uses a series of spectral bands in addition to individual retrievals of physical quantities, such as the difference between retrieved above-cloud precipitable water amounts from the 0.94 μm band and from the CO_2 slicing cloud top height, and cloud optical thickness difference between the standard retrieval at 2.1 μm channel and the alternative 1.6–2.1 μm channel pair, to decide the existence of multilayer clouds. However, CALIOP discriminates the layers as multilayer clouds if individual layers are always separated by regions of “clear air”, and layer boundaries never overlap each other in the vertical dimension. By comparing the combined cloud layer dataset from CloudSat/CALIPSO with MODIS cloud multilayer flag, some studies have indicated that MODIS usually underestimates the multilayer clouds ([Li et al., 2011b](#); [Wang et al., 2016](#)). Recent, [Sun-Mack et al. \(2017\)](#) utilized an artificial neural network algorithm to train the brightness temperatures at several MODIS infrared channels and the retrieved total cloud visible optical depth, in order to detect multilayer ice-over-water cloud systems as identified by collocated CloudSat/CALIPSO cloud product. Their results exhibit higher accuracy than currently available methods. As a result, we use the combined information from the “cloud layer number” of CALIPSO and “cloud multilayer flag” of MODIS to double-check the multilayer clouds in order to minimize their effects. It will not affect our statistical results except reduce the sample numbers.

Here, two points still require further interpretation. First, because lidar signal of CALIOP can be completely attenuated when cloud optical depth (τ) exceeds CALIOP’s detection limit of effective optical depth ($\eta\tau < 3$, η is multiple scattering factor) ([Hu et al., 2007b](#)), CALIOP can’t penetrate the optically thick cloud layers to detect the lower cloud layers. In the circumstances, CALIOP still reports the “cloud layer number” as 1 so that some multilayered cloud systems are mistaken for single-layer clouds. Although the limitation of the “cloud layer number” will not bias the retrieval N_d to thin water clouds, the misclassification of “cloud layer number” may still cause some uncertainties in our results. Second, CALIOP only can penetrate limited depth of cloud layer,

thus the consideration of “liquid phase cloud” only focuses on the cloud phase of very top part of clouds. It means that some liquid-layer topped mixed-phased clouds are also included in our statistical samples, especially for supercooled water clouds. But, it will not affect our results because the retrieval N_d based two methods are both in the top part of clouds. Meantime, it is worth noting that the cloud top temperatures of clouds in our study range from -30°C to 30°C .

In addition, current satellite observations still have difficulty to derive the information of aerosol and vertical velocity at the cloud base, thus we also extract the vertical profiles of the averaged vertical velocity w from MERRA2 and ERA-interim reanalysis and aerosol mass mixing ratios from MERRA2 closest to the CALIPSO observations in both space and time. It means that the vertical velocity used in this investigation refers to the large-scale vertical motion and differs from the values of the updraft velocities at the cloud base or in the clouds mentioned in previous studies ([Reutter et al., 2009](#); [Rosenfeld et al., 2016](#)). For each cloud sample, only velocity and aerosol concentration near cloud base in their profiles are used in following analysis since the aerosols that serve as cloud condensation nuclei generally get into clouds from cloud bases ([Zhao et al., 2018](#)). Note that we limit our analysis to $\pm 60^\circ$ latitudes, a low solar zenith angle ($< 65^\circ$) and a high MODIS cloud fraction ($> 80\%$) within a spatial resolution at $5 \times 5 \text{ km}$ to reduce the statistical uncertainty caused by the retrieval biases of the cloud properties (e.g., the effective radius at 3.7 μm will be strongly biased at high solar zenith angle) ([Bennartz and Rausch, 2017](#); [Grosvenor and Wood, 2014](#)).

Given these screening criteria, the two retrieval algorithms both perform at a pixel-level and the number of available samples is at least one hundred million, thus ensuring the statistical significance. Here, it is worth noting that the global distributions and seasonal cycles of N_d in [Fig. 2](#) are the 10-year averaged values; thus, the grid size of N_d is set as 2° latitude by 2° longitude. In view of the current study mainly focuses on the roles of aerosol types and larger-scale updrafts in the temporal variability of the regional and global N_d , all pixel-level variables are further collected to establish the long-term gridded datasets of seasonally averaged variables. To do this, we enlarge the grid size as 2° latitude by 3° longitude to avoid the issue of a sparse dataset caused by the narrow orbit of CALIOP, and to provide enough long time series of different parameters in each grid to build a robust multiple linear regression model.

Using the samples (see the [Fig. 1](#)), we have showed the impact of multilayer clouds on the retrievals of N_d . To facilitate comparisons, the latest N_d dataset from the Aqua-MODIS measurements spanning the

years from 2007 to 2015 is also used in our investigation (Bennartz and Rausch, 2017; data link: <https://doi.org/10.15695/vudata.ees.1>). The improved dataset still includes multilayer clouds, thus, is a good reference to assess the effects of multilayer clouds. Comparisons are performed for two different regions: the western coast of North America (114–128°W; 17–32°S) and the eastern coast of North America (70–60°E; 35–45°S). In Fig. 1, the MODIS-single and MODIS-all datasets represent the single-layered and all liquid warm water clouds, respectively. The western coast of North America is a typical subtropical stratocumulus region where multilayered clouds are very scarce due to subsidence (Li et al., 2015). For the N_d anomalies (that is, $\Delta\log_{10}(N_d)$), Fig. 1a clearly shows that the three N_d datasets exhibit high consistencies and their correlations all exceed 0.8. Note that the anomalies of all variables in this study are already deseasonalized. Over the eastern coast of North America (multilayered clouds account for 30% to 40% of the total cloud fraction) (Li et al., 2015), however, the consistency is reduced. Comparing Fig. 1b with Fig. 1a, we can see that the correlation coefficient between MODIS-all and MODIS-single drops from 0.81 to 0.66, and the correlation coefficient between CALIPSO and MODIS-all drops from 0.84 to 0.6. However, CALIPSO and MODIS-single still show a good agreement. Although the above result cannot be entirely ruled out as being due to the effects of other factors (e.g., different screening criteria used in two MODIS datasets), the bias from multilayered clouds is still non-negligible (Ahmad et al., 2013). As a result, the following analysis is based only on the CALIPSO and MODIS-single N_d datasets. Recent, some studies have verified the validity of the MODIS retrieval method by using aircraft measurements (Bennartz and Rausch, 2017; McCoy et al., 2017c). However, it is difficult to directly evaluate the CALIPSO retrieval in the present study due to its narrow orbit and the scarcity of aircraft observations. Here, we also find that the variations of $\Delta\log_{10}(N_d)$ from CALIPSO almost are synchronous with the variations of depolarization ratio anomalies ($\Delta\delta$), whereas effective radius anomalies ΔR_e have relative lower but negative correlation with $\Delta\log_{10}(N_d)$ from CALIPSO retrieval (see the Fig. S1 in the Supplementary material).

3. Results and discussion

3.1. Global and regional comparisons of two N_d climatological datasets

Fig. 2 shows the global distributions of the ten-year average retrieved N_d values for different boreal seasons with a $2^\circ \times 2^\circ$ grid. The left panel depicts the results from CALIPSO, and the right panel shows those from MODIS. We find that the global distributions of N_d are very similar for the two methods. The cloud droplet number concentration is generally large over landmasses (e.g., northern and eastern China, eastern America, South Africa, and Europe) and significantly lower over remote oceans, especially over the tropical cumulus regions, where the N_d is almost lower than 40 cm^{-3} . The maximum values of N_d can reach 200 and 300 cm^{-3} for CALIPSO and MODIS, respectively. Overall, the global mean N_d derived from the CALIPSO retrieval are approximately 52, 51, 53, 56 and 53 cm^{-3} for the spring, summer, autumn, winter and annual means, respectively. The corresponding values derived from the MODIS retrieval are 110, 108, 114, 129 and 114 cm^{-3} . Based on these statistical results, it is clear that the global mean N_d from the MODIS retrieval is approximately 2 times greater than that of the CALIPSO retrieval. At the regional scale, the difference in the N_d values of the two methods is much greater than that of the global means, especially over the cumulus region for the whole year or over the Southern Ocean during the boreal summer season. For the typical subtropical stratocumulus regions (such as, the Californian, Canarian, Namibian regions), the differences are relatively small, especially during the summer (see the Fig. S2 of the Supplementary information). Here, it is worth noting that the ratio between N_d from MODIS and CALIPSO methods in the Fig. S2 is independent on the cloud droplet size distribution parameters due to same γ values are used. Thus, the obvious regional distribution rate of the N_d of MODIS and CALIPSO may be partly linked to the feasibility of adiabatic assumptions for different cloud regimes. Some previous studies have shown that stratocumulus clouds tend to be adiabatic (Albrecht et al., 1990; Zuidema et al., 2005); thus, the MODIS method may exhibit a relatively reliable retrieval of N_d over these

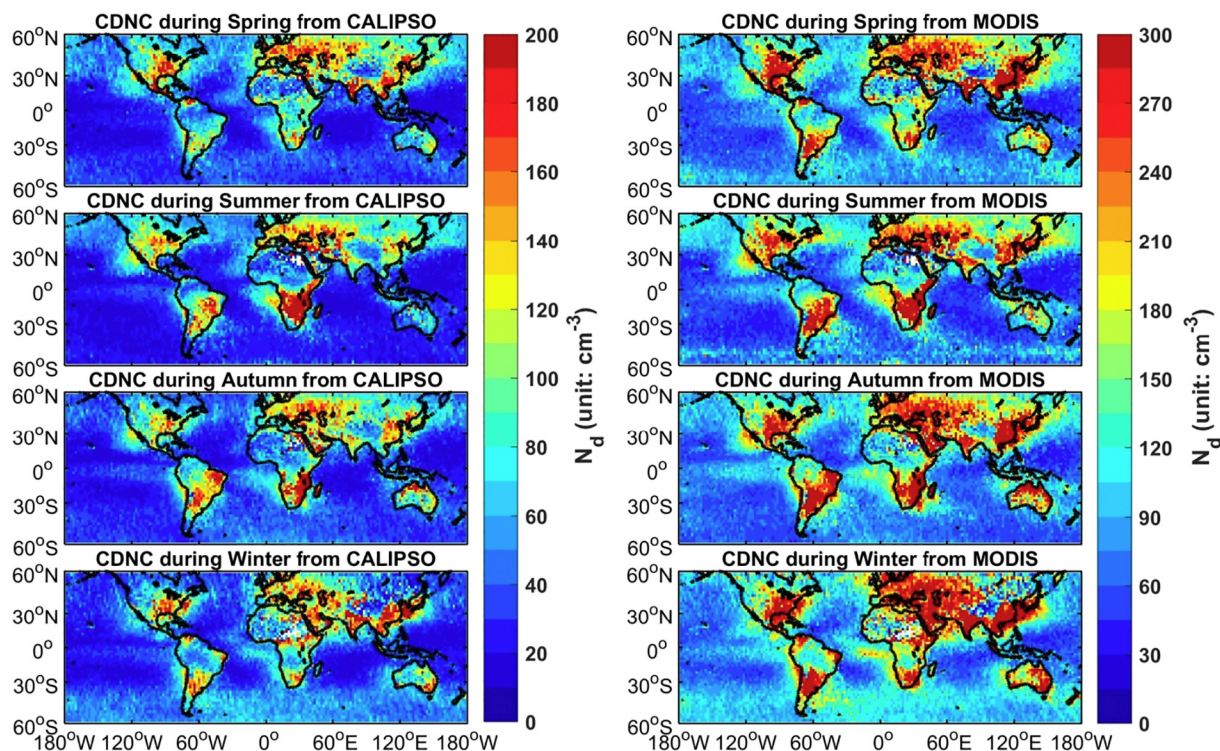


Fig. 2. The global distributions of ten years average retrieved N_d for different boreal seasons in a $2 \times 2^\circ$ grid box. The left panel depicts the results from CALIPSO and the right panel is for the MODIS.

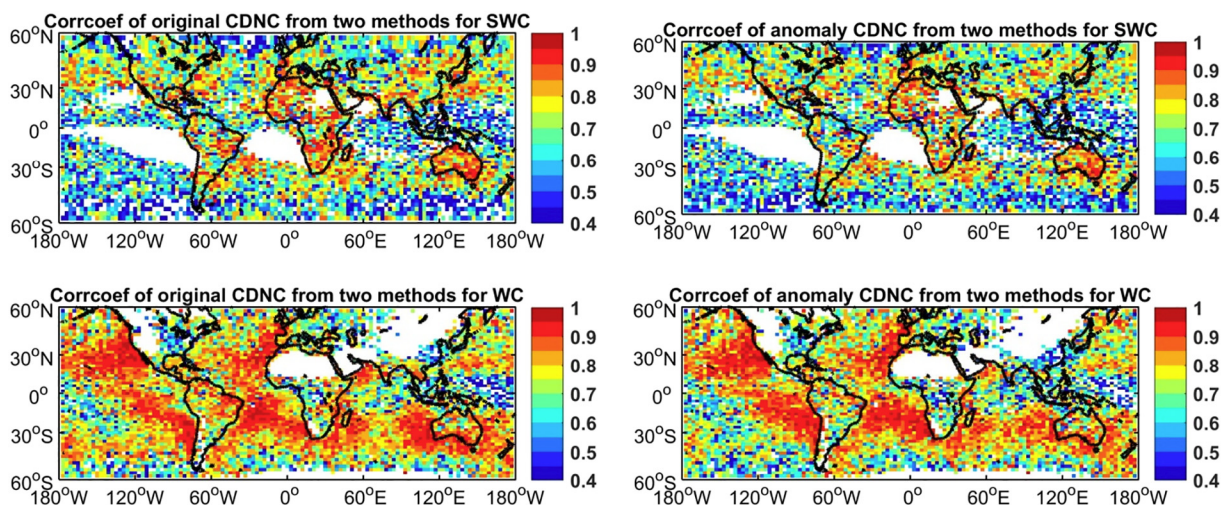


Fig. 3. The global distributions ($2 \times 3^\circ$ grid box) of temporal correlation coefficients of N_d (and its anomaly) between MODIS and CALIPSO methods. Specifically, left column corresponds to correlation coefficient of original N_d time series for supercooled water clouds (SWC, upper panel) and warm water clouds (WC, lower panel). The right column corresponds to the correlation coefficient of anomaly N_d time series for supercooled water clouds (SWC, upper panel) and warm water clouds (WC, lower panel).

stratocumulus regions (Bennartz and Rausch, 2017). The comparison of cloud liquid water path based on the Advanced Microwave Scanning Radiometer-EOS (AMSR-E) retrieval and MODIS calculations, which rely on a typical adiabatic model, also reveals that the best agreement occurred in the extensive marine stratocumulus regions off the west coasts of land masses, which showed correlations of 0.95 and RMS differences of 15 g m^{-2} (Seethala and Horváth, 2010). Indeed, by performing a temporal correlations analysis, we also find that the MODIS and CALIPSO retrievals are most consistent in the stratocumulus regions, for both N_d and its anomaly (see Fig. 3), although some differences still exist due to the entrainment process at the cloud top, which shows unsaturated environmental air entrained in the clouds diluting and evaporating the droplets and may result in a decrease in r_e and N_d at the cloud top (Wood, 2012). Overall, it is still hard to determine which method provides the most accurate N_d retrievals based only on current study; however, similar global and seasonal distributions give us confidence to further discuss the consistency of long-term variations between two N_d climatologies.

Note that the statistical results in Fig. 2 are from all liquid water cloud samples. Existing studies of N_d based on MODIS retrievals mainly focus on warm water clouds, which have typical cloud top temperatures between 268 and 300 K (Bennartz and Rausch, 2017). An accurate determination of supercooled water clouds remains problematic for the MODIS collection-6 IR phase algorithm (Baum et al., 2012), although the clouds of such phase have been found to be poorly simulated in the global climate models, especially over the Southern Ocean (Morrison et al., 2011; Trenberth and Fasullo, 2010). In fact, the possible differences between warm and supercooled clouds discrimination from CALIPSO and MODIS cloud phase algorithms mainly reflect the uncertainty on the discrimination between liquid and mixed-phase clouds in the case of super-cooled water clouds based on passive sensors (Cho et al., 2009; Baum et al., 2012). In view of the sensitivity of CALIPSO to the cloud top phase, this study utilizes the cloud phase and top temperature information from CALIPSO to divide the cloud samples into warm and supercooled water clouds. Specifically, we consider the water clouds as warm (or supercooled) water clouds if their cloud top temperatures are higher than 0°C (or -30°C) and lower than 30°C (or 0°C).

Fig. 3 shows the global distributions of the temporal correlations of N_d (and its anomaly) between the MODIS and CALIPSO methods for warm and supercooled liquid water clouds. Those regions without data indicate that the data of the N_d time series in this grid are smaller than

20 and, thus, are replaced with a default value. Obviously, the global distributions of the temporal correlations of N_d and its anomaly are very similar. Compared with supercooled water clouds, the N_d values of warm water clouds have much higher temporal correlations (even reach 0.9), especially over the stratocumulus regions. Generally, large temporal correlations for supercooled water clouds are located over landmasses, whereas obvious correlations of warm water clouds mainly exist over the ocean.

Here, we also present regional comparisons of the mean N_d annual cycle and the seasonal N_d anomalies from the two methods (Figs. 4, 5 and 6) for different regions. The statistical results in each region are also provided in Table 1. For clarity, we take region 1 panel as an example to explain what each plot is, especially the means of each legend, color, symbol and label. The bars in the figure (a) of region 1 represent the annual cycle of N_d of warm water clouds from CALIPSO (black color) and MODIS (white color) methods. The normalized annual cycle value is represented as the ratio of the monthly means to their maxima. In the figure (a), we also provide the correlation coefficients (and confidence level p) of annual cycle of N_d between two methods for warm (red color) and supercooled water clouds (black color), respectively. Figure (b) in the region 1 shows the location of selected region. Further, figure (c) gives the long-term variations of N_d anomaly from CALIPSO (red line) and MODIS (black line) retrievals for warm water clouds ($0^\circ\text{C} < \text{cloud top temperature} < 30^\circ\text{C}$). The correlation coefficient of time series of N_d anomaly between two methods is given in the figure (c). In addition, the annual averaged values of N_d from CALIPSO (MODIS) methods are also provided. Same as the figure (c), the figure (d) in the region 1 gives the long-term variations of N_d anomaly from CALIPSO (cyan line) and MODIS (black line) retrievals for supercooled water clouds ($-30^\circ\text{C} < \text{cloud top temperature} < 0^\circ\text{C}$).

For the annual cycle of warm water clouds (that is, bar plots), the two N_d datasets in most of regions show similar monthly variations (correlation coefficient R may exceed 0.7) at high confidence levels ($> 95\%$) except over the eastern coast of America (region 2, $R = -0.06$) and western coast of South Africa (region 11, $R = 0.51$). The monthly variations of N_d obviously differ from region to region. N_d is highest during the boreal summer and lowest in the winter for South Africa (region 3), whereas the lowest N_d occurs in the boreal summer over the eastern part of Australia (region 4). Furthermore, the monthly variations in some region are also opposite those of the adjacent regions (e.g., region 6 vs region 11). This pattern may be linked to the seasonal variations of different aerosol types and their concentrations. For

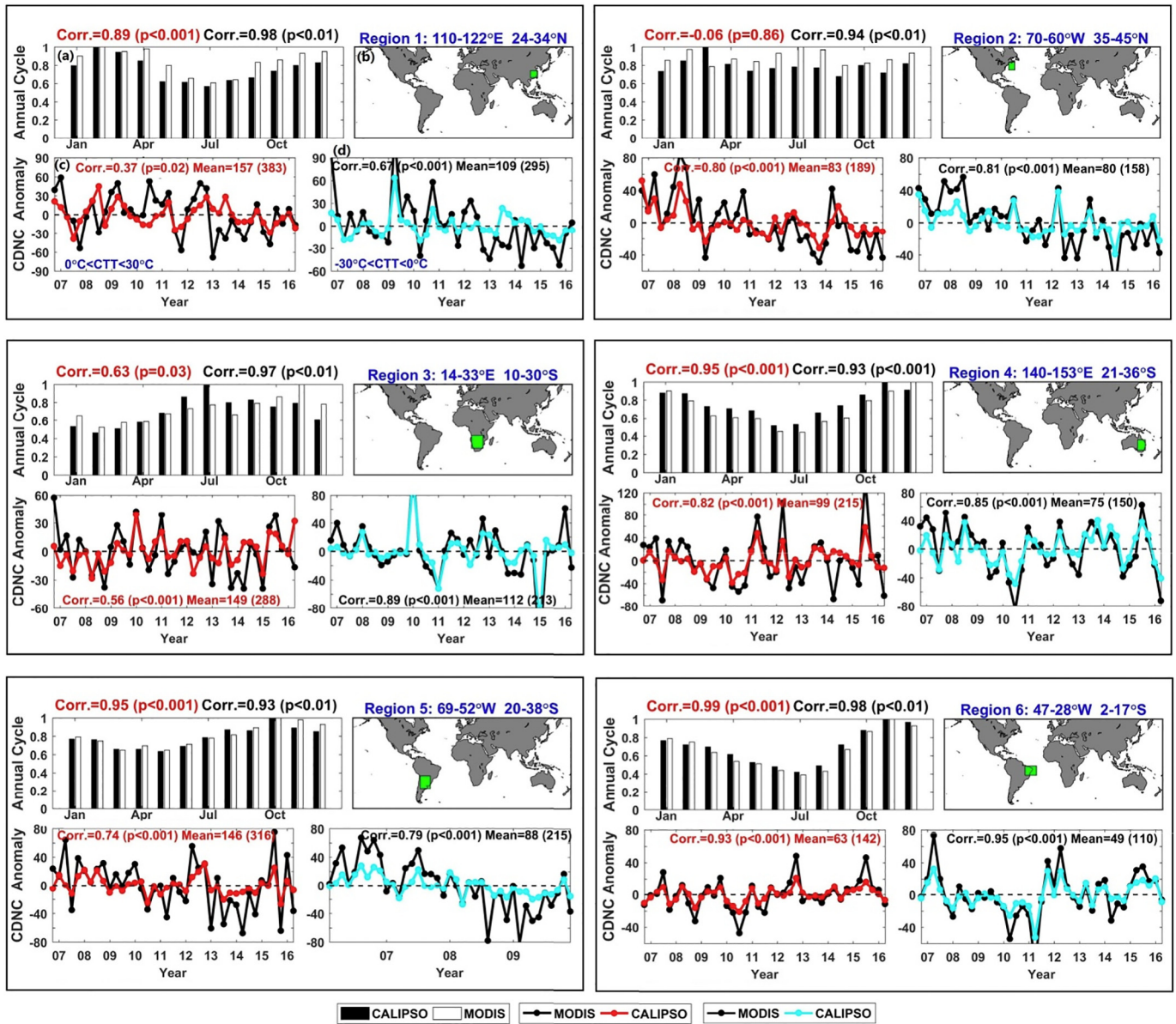


Fig. 4. Regional comparisons about averaged N_d annual cycle and long-term variation of seasonal N_d anomalies between two methods for region 1–region 6. The bar plot (left-up plot) represents the annual cycle of N_d of warm water clouds; We also provide the correlation coefficients of annual cycle of N_d between two methods for warm water clouds (red color) and supercooled water clouds (black color) and their confidence level (p value). The Map (right-up plot) shows the studied region (green box). In the left-down subplot, the black and red lines represent the time series of N_d of warm water clouds from MODIS and CALIPSO, respectively. Similar, in the right-down subplot, the black and cyan lines represent the time series of N_d of supercooled water clouds from MODIS and CALIPSO, respectively. Besides the correlation coefficients between time series of N_d . In the two subplots, regional averaged N_d from CALIPSO (MODIS) for warm (red color) and supercooled water clouds (black color) are also provided. Table 1 provides the detailed information. (For interpretation of the references to color in this figure legend, the reader is referred to the web version of this article.)

example, Bennartz and Rausch (2017) indicated that the biomass burning during September in southeastern Africa and Madagascar is consistent with the peak value of N_d in the eastern part of South Africa, whereas McCoy et al. (2015) found that the annual cycle of N_d is driven mainly by high concentrations of sulfate aerosols at the lower Southern Ocean latitudes (35–45°S) and by organic matter in sea spray aerosols at the higher latitudes (45–55°S). For the Southern Ocean (regions 16 and 17), we find that the N_d from the MODIS method has two peaks during May/June and December/January, which are consistent with the results from Bennartz and Rausch (2017). However, in situ measurements of CCN in the Southern Ocean show only one peak, with a boreal winter maximum and boreal summer minimum (Gras, 1990; Gras and Keywood, 2017). Compared with MODIS, our results from the CALIPSO method agree well with the annual cycle of the CCN

measurements in the Southern Ocean for both warm water clouds and supercooled water clouds. The annual cycles of supercooled water clouds are similar to those of warm water clouds in most regions, except for regions 11, 12 and 15 (figure not shown).

The time series of the seasonal N_d anomalies also show better consistencies between two methods. In Figs. 4, 5 and 6, it is clear that the N_d of the supercooled water clouds is obviously lower than that of warm water clouds, especially over the stratocumulus regions. The decrease of N_d with decreasing of cloud top temperature agrees with the vertical variation of the depolarization ratio with water cloud top temperature, which might be caused by the fact that the cloud mean liquid water content or liquid water paths for clouds with the same thicknesses decrease when cloud temperature decreases (Li et al., 2011a). Over these remote oceans (e.g., regions 10, 16 and 17), which are less affected by

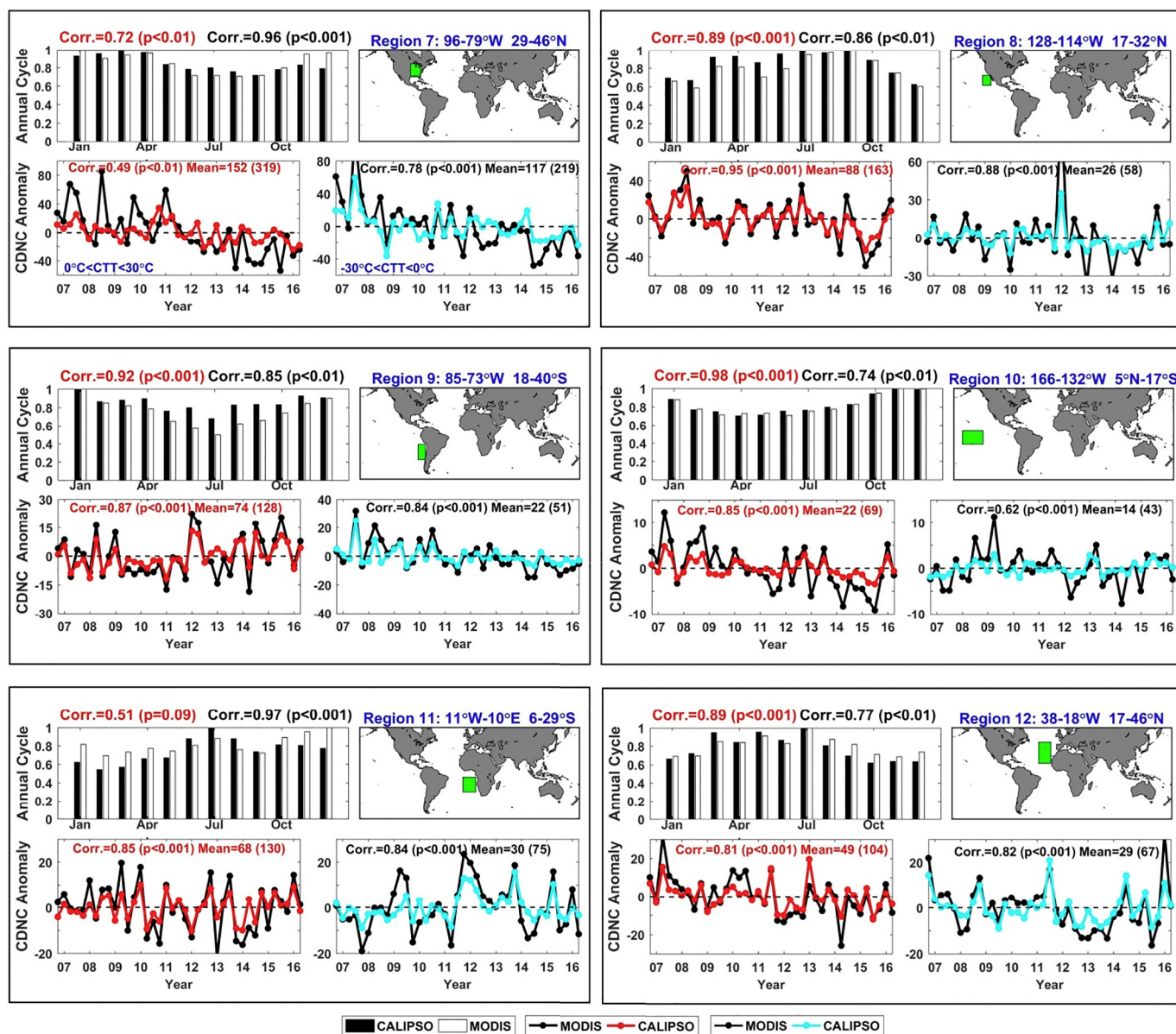


Fig. 5. Same as Fig. 4, except for regions 7–12.

anthropogenic aerosols, statistical results show relatively stable and small anomalies for CALIPSO retrievals (anomalies smaller than $\pm 10 \text{ cm}^{-3}$). However, the seasonal N_d anomalies from the MODIS retrieval show slight decreasing trends, especially for region 17. From Table 1, we can see that the trend reaches $-15 \text{ cm}^{-3}/10 \text{ yrs}$ for supercooled water clouds in region 16, and -14.8 and $-13.8 \text{ cm}^{-3}/10 \text{ yrs}$ for the warm and supercooled water clouds, respectively, in region 17. These results are inconsistent with the recent study from Bennartz and Rausch (2017), which used the individually MODIS retrievals to analyze the monthly N_d anomalies in similar regions and did not find any serious trends. By comparing the results from MODIS over other regions (e.g., region 2: eastern part of America), this study also finds a very obvious decreasing trend ($-67 \text{ cm}^{-3}/10 \text{ yrs}$) consistent with that of study from Bennartz and Rausch (2017) ($-50 \text{ cm}^{-3}/10 \text{ yrs}$). This result means that the inconsistencies over the Southern Ocean could not be retrieval errors in our study because these two studies use similar MODIS data and retrieval methods. One of the possible reasons is that the different screening criteria are used in our study, but this will be further examined in a later study. For those polluted regions (e.g., region 1: eastern part of China), the mean N_d for the warm and supercooled water

clouds from MODIS (or CALIPSO) reaches 383 (or 157) cm^{-3} and 295 (or 109) cm^{-3} , respectively. However, the long-term variations of the seasonal N_d anomalies do not exhibit statistically significant trends, excepting the supercooled water clouds from the MODIS retrieval. However, it is interesting to see that N_d in the area adjacent to region 1 (that is, region 15: East China Sea) exhibits an obvious negative trend for the MODIS and CALIPSO methods (-47.6 vs $-14.3 \text{ cm}^{-3}/10 \text{ yrs}$). This conclusion is opposite to the results of the previous study from Bennartz et al. (2011), which used the satellite retrieval and model simulation to show an increasing trend of N_d from $< 200 \text{ cm}^{-3}$ in the 1980s to $> 300 \text{ cm}^{-3}$ in 2005. In view of the difference of observation periods, Bennartz and Rausch (2017) attributed the inconsistent trend to the introduction of flue gas desulfurization technology in Chinese factories, which resulted in a significant decline of the SO_2 emissions in recent years compared to those of the peak emission year (e.g., approximately 2006) (Klimont et al., 2013; Krotkov et al., 2016; He et al., 2017). Similarly, a significantly negative trend of N_d was observed over the eastern part of America (region 7) and is also captured by the MODIS and CALIPSO retrievals for both warm or supercooled water clouds; the MODIS (CALIPSO) values are -73.8 (-26.1) $\text{cm}^{-3}/10 \text{ yrs}$

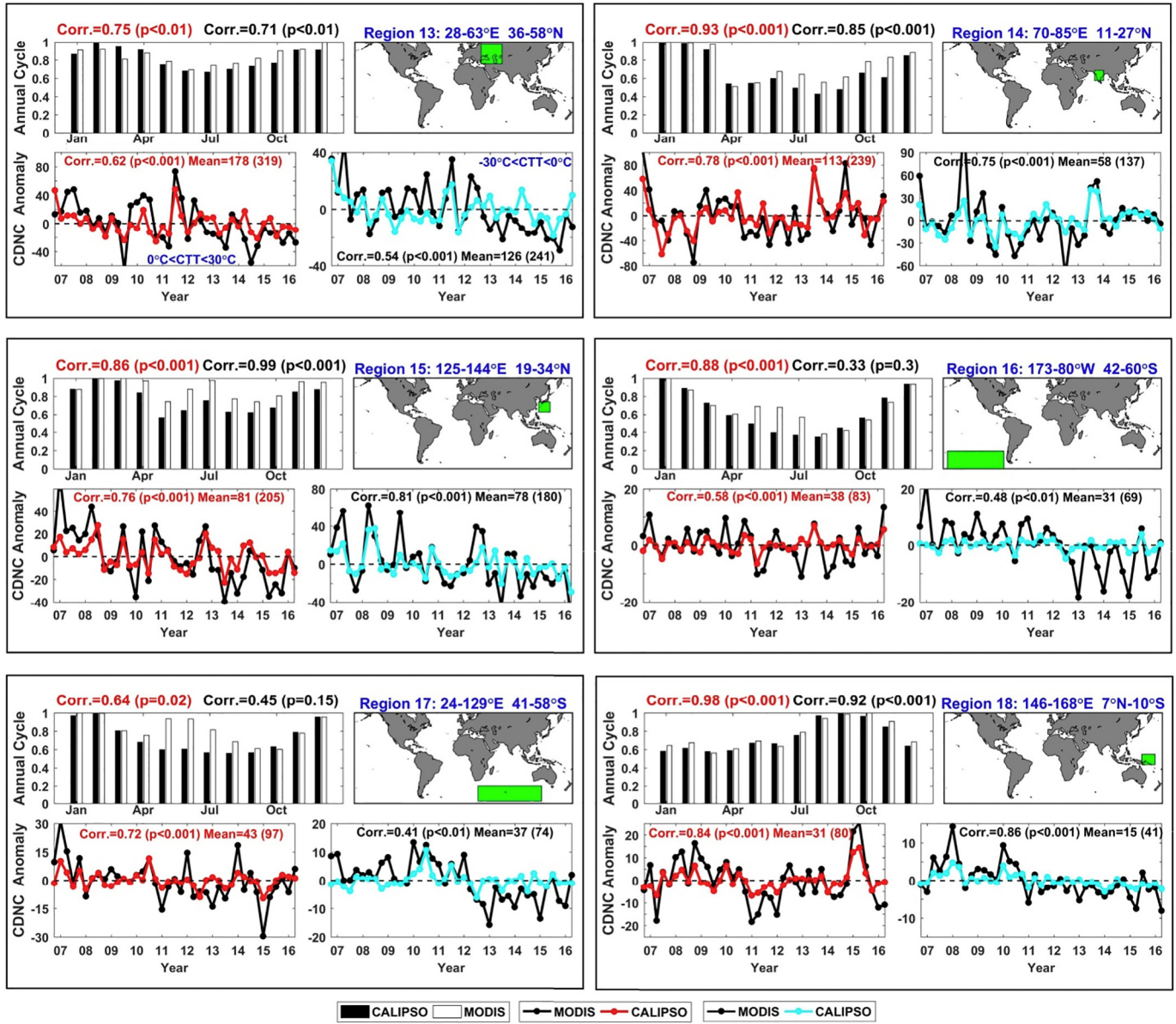


Fig. 6. Same as Fig. 4, except for regions 13–18.

and $-61.4 (-27.1) \text{ cm}^{-3}/10 \text{ yrs}$ for the warm and supercooled water clouds, respectively. Finally, the two N_d datasets both exhibited weak but still significant negative trends for the globally averaged N_d , and the N_d of the supercooled water cloud drops more quickly than those of the warm water clouds (see region 19 in the Table 1). Such changes of N_d have been proven to have important impacts on the reflected shortwave radiation and precipitation frequencies of clouds on regional and global scales (Bennartz et al., 2011; Hoose et al., 2009; McCoy et al., 2015, 2017b).

3.2. Regression modeling and contribution calculation

How can we better understand the factors that drive the long-term variations of N_d in different regions? What factor is the dominant? This study builds a regression relationship between the N_d , the mass concentrations of different aerosol species and the atmospheric vertical velocity in order to eventually quantify the relative contributions of different factors to the observed variability of N_d . Similar to the study from McCoy et al. (2017b), the basic multiple linear regression model is given as:

$$\begin{aligned} \Delta \log_{10}(N_d) = & a_1 \times \Delta \log_{10}(SO_4) + a_2 \times \Delta \log_{10}(SO_2) + a_3 \times \Delta \log_{10}(OC) \\ & + a_4 \times \Delta \log_{10}(BC) \\ & + a_5 \times \Delta \log_{10}(DU) + a_6 \times \Delta \log_{10}(SS) + a_6 \times \Delta w + b \end{aligned} \quad (5)$$

where all variables are deseasonalized anomalies; and the units of N_d , aerosol mass concentrations and vertical velocity are cm^{-3} , $\mu\text{g}/\text{m}^3$ and hPa/h , respectively. a_n is the regression coefficient for the different predictors and b is the constant term. The regression models based on the MODIS and CALIPSO N_d datasets are trained separately in every selected region by using an aggregated grid ($2 \times 3^\circ$) of the seasonal anomalies in these regions. Here, it is noted that the collinearities of different predictor variables need to be tested before building regional regression models. For those regions without collinearities, the variables are considered as predictors when the time series of their seasonal anomalies show significant correlation (confidence level $> 95\%$) with the seasonal anomalies of N_d . For those regions with collinearity, the stepwise regression method is used to filter the predictors and build regression models.

Fig. 7 plots all regression coefficients in the models for different

Table 1

Detailed information about the boundaries of regions, regional means, correlation coefficient and trends of N_d for warm water clouds (WC) and supercooled water clouds (SWC).

Reg.	Lat. °N (upper/lower)	Lon. °E (left/right)	Mean ^a (WC) cm ⁻³	Mean (SWC) cm ⁻³	Corr. ^b (time series)	Corr. ^c (annual cycle)	Slope ^d MODIS cm ⁻³ /10 yr	Slope CALIPSO cm ⁻³ /10 yr
R1	34/24	110/122	157 (383)	109 (295)	0.37 (0.67)	0.89 (0.98)	– (–39.3)	– (–)
R2	45/35	–70/–60	83 (189)	80 (158)	0.8 (0.81)	– (0.94)	–66.7 (–65.3)	–20.4 (–23.2)
R3	–10/–30	14/33	149 (288)	112 (213)	0.56 (0.89)	0.63 (0.97)	– (–)	– (–)
R4	–21/–36	140/153	99 (215)	75 (150)	0.82 (0.85)	0.95 (0.93)	– (–)	– (–)
R5	–20/–38	–69/–52	146 (316)	88 (215)	0.74 (0.79)	0.95 (0.93)	–48.8 (–83.4)	– (–27.5)
R6	–2/–17	–47/–28	63 (142)	49 (110)	0.93 (0.95)	0.99 (0.98)	– (–)	– (–)
R7	46/29	–96/–79	152 (319)	117 (219)	0.49 (0.78)	0.72 (0.96)	–73.8 (–61.4)	–26.1 (–27.1)
R8	32/17	–128/–144	88 (163)	26 (58)	0.95 (0.88)	0.89 (0.86)	– (–)	–21 (–)
R9	–18/–40	–85/–73	74 (128)	22 (51)	0.87 (0.84)	0.92 (0.85)	– (–16)	9.7 (–5.5)
R10	5/–17	–166/–132	22 (69)	14 (43)	0.85 (0.62)	0.98 (0.74)	–9.5 (–)	– (–)
R11	–6/–29	–11/10	68 (130)	30 (75)	0.85 (0.84)	– (0.97)	– (–)	– (–)
R12	46/17	–38/–18	49 (104)	29 (67)	0.81 (0.82)	0.89 (0.77)	–16.6 (–12.3)	–6.5 (–)
R13	58/36	28/63	178 (319)	126 (241)	0.62 (0.54)	0.75 (0.71)	–49.2 (–36.6)	– (–)
R14	27/11	70/85	113 (239)	58 (137)	0.78 (0.75)	0.93 (0.85)	– (–)	– (–)
R15	34/19	125/144	81 (205)	78 (180)	0.76 (0.81)	0.86 (0.99)	–47.6 (–39)	–14.3 (–)
R16	–42/–60	–173/–80	38 (83)	31 (69)	0.58 (0.48)	0.88 (–)	– (–15)	– (–)
R17	–41/–58	24/129	43 (97)	37 (74)	0.72 (0.41)	0.64 (–)	–14.8 (–13.8)	– (–)
R18	7/–10	146/168	31 (80)	15 (41)	0.84 (0.86)	0.98 (0.92)	– (–9.3)	– (–3.3)
R19	60/–60	–180/180	56 (121)	47 (101)	0.39 (0.63)	0.64 (0.91)	–10.4 (–18.2)	–1.6 (–3.1)

^a Represent the regional averaged N_d of WC for CALIPSO (MODIS) methods.

^b Correlation coefficient between CALIPSO and MODIS methods for the time series of seasonal N_d anomalies of WC (SWC); “–” represent the confidence level < 95%.

^c Correlation coefficient between CALIPSO and MODIS methods for the annual cycle of N_d of WC (SWC); “–” represent the confidence level < 95%.

^d Trend of N_d based on MODIS and CALIPSO retrievals for WC (SWC); “–” represent the confidence level < 95%.

regions (see the detailed information in the Tables 2 and 3). In these regression models, the constant term b is almost equal to zero; thus, its information is not provided in Fig. 7 or Tables 2 and 3. In Fig. 7, we can see that the coefficients almost remain positive for SO_2 and SO_4 for both supercooled and warm water clouds. On average, the coefficients of SO_4 are higher than those of other variables. The results are consistent with those of the study from McCoy et al. (2017b), which also noted that the SO_4 explained a large fraction of the variability of N_d . The coefficients of SO_2 in the models reveal similar sensitivities of different N_d retrieval datasets to SO_2 , although differences are still obvious in some regions. Compared with the results of SO_4 and SO_2 , it is interesting to note that the coefficients of the other aerosol types exhibit unexpected negative values in some of the study regions, especially for BC and OC. McCoy et al. (2017c) also found negative dependence of N_d on BC and OC in some select regions and attributed these to the uncertainty of the MERRA2 reanalysis and semi-direct aerosol effect. Indeed, Bennartz and Rausch (2017) evaluated the impacts of biomass burning aerosols over clouds on the retrievals of N_d . They found that the retrieved effective radii (or cloud optical depth) from passive sensors will increase (or decrease) when increasing the optical depths of the absorbing aerosols. This eventually results in a decrease in the retrieved N_d and

provides a possible interpretation of the negative dependence of N_d on BC. The effectiveness of OC as CCN has been verified in previous studies (e.g., Novakov and Penner, 1993). However, by compiling the CCN activity of water-soluble organic carbon (WSOC) from existing studies, Ervens et al. (2005) found the predicted relative changes in N_d caused by WSOC produce ambiguous results regarding the magnitude and even the sign of the change (e.g., have a wide range from –86% to 110%). This work showed that the inconsistent changes of N_d stemmed from physicochemical properties of WSOC, such as the solubility, surface tension and molecular weight. This finding may partially explain the negative sensitivities of N_d to OC over some regions. For submicron sea salt and dust aerosols, our results also exhibit negative but relatively weaker dependences over several regions. Compared with the coefficients from the CALIPSO method, the sensitivities of N_d from MODIS to SS show more negative values, especially for the warm water clouds over regions 13–18. Some studies have attributed these results to the impacts of meteorological factors on N_d because the sea salt in MERRA2 is generated from the wind speed and sea surface temperature based on a simple parameterization (Grythe et al., 2014; McCoy et al., 2017b).

In the present study, we also test the sensitivity of N_d to vertical velocity. Model simulations have shown positive correlations between

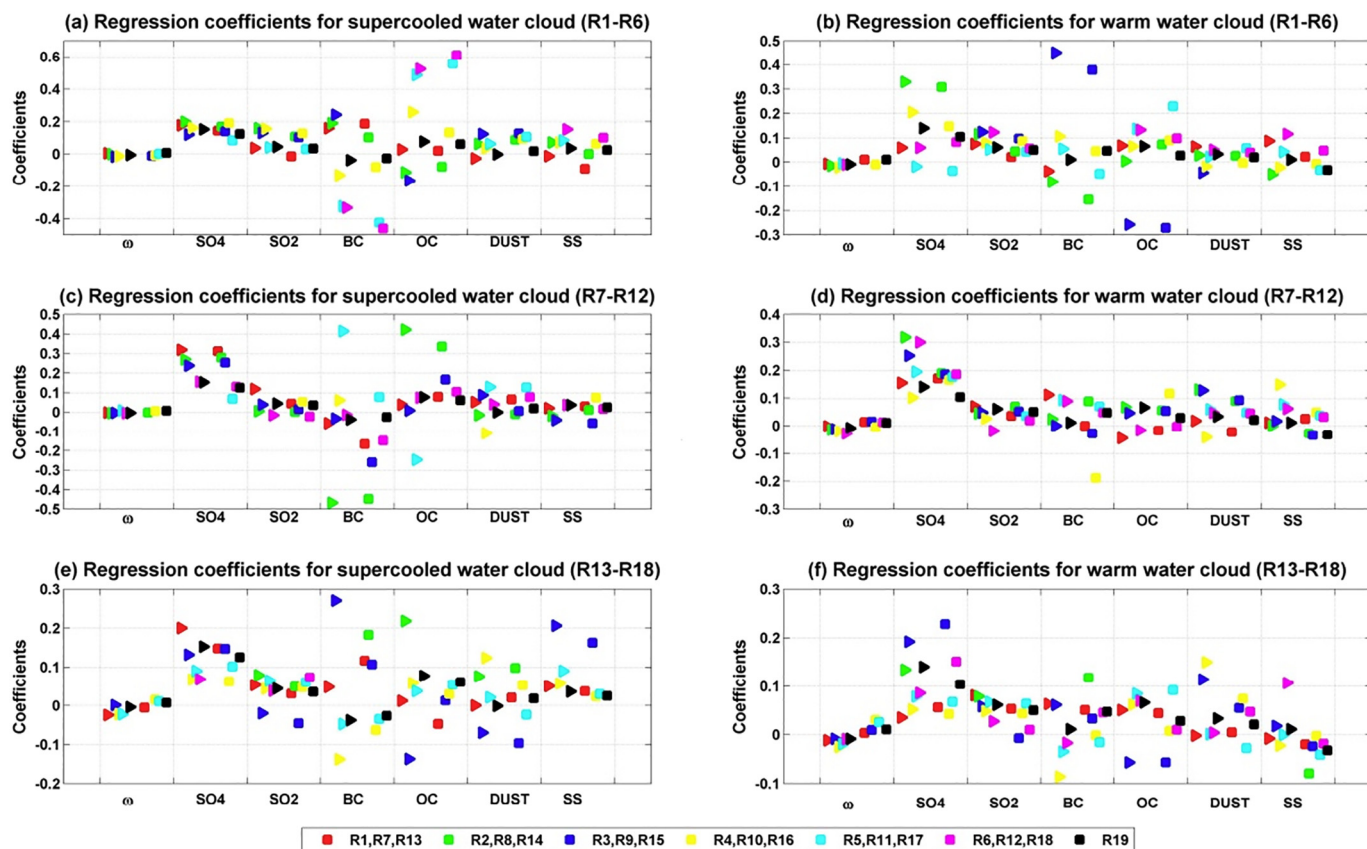


Fig. 7. The regression coefficients of different predictors in the regression models. The square and triangle symbols represent the results from MODIS and CALIPSO datasets, respectively. Tables 2 and 3 provide the detailed information.

in-cloud updrafts and N_d because high in-cloud updrafts may lead to maximum supersaturations large enough to activate most of the aerosol particles, except those of very small particles (Reutter et al., 2009). Some studies also verified in-cloud updraft enhancement can lead to an increase of the liquid water path (West et al., 2014) and the growth of liquid water in the Arctic mixed-phase clouds (Shupe et al., 2008). Our results show a negative but weak sensitivity of N_d to ω (Fig. 7). However, we should note that the vertical velocity used in our investigation refers to the average large-scale vertical motion from the two reanalysis datasets and is different from the updraft velocity in clouds or at cloud bases mentioned in previous simulation studies (Karydis et al., 2012; Reutter et al., 2009; Sullivan et al., 2016). Although some observational studies demonstrated that a strong large-scale ascent motion suppresses the formation of supercooled water clouds (Cesana et al., 2015; Li et al., 2017), few researches have addressed the impact of large-scale ascent motions on cloud droplet number concentrations. We speculate that the negative sensitivity of N_d to ω might be because the large-scale ascent in this study smooths out many of the cloud-scale vertical motions. Another possible reason is that the strong large-scale ascent may lift larger cloud droplets and result in a relatively smaller N_d for a given the liquid water path.

By using the regression model in each region, we also calculate the anomalies of $\log_{10}(N_d)$ in each grid for these regions and further derive the regressed regional averaged anomalies of $\log_{10}(N_d)$. Fig. 8 indicates the correlation coefficients between the observed and regressed regionally averaged $\Delta\log_{10}(N_d)$ in different regions for supercooled and warm water clouds, respectively. It is clear that the correlation coefficients based on the CALIPSO N_d dataset are systemically higher than those of the MODIS retrieval for both supercooled and warm water clouds except in a few regions (e.g., the Southern Ocean regions). This result means that the CALIPSO N_d retrieval method along with the regression model has the ability to reproduce long-term variations of the

regional averaged N_d .

Figs. 9 and 10 show the time series of the regional means of the regressed and observed $\Delta\log_{10}(N_d)$ in some selected regions. Based on the regression coefficients, the combined time series of the two main predictors are also provided in Figs. 9 and 10. For the warm water clouds in region 2 (eastern coast of America), although the regressed $\Delta\log_{10}(N_d)$ is systemically smaller than the observed values, its long-term variations agree well with the observed time series from CALIPSO and MODIS. The correlation coefficients reach 0.73 and 0.69, respectively. Based on the negative trend of N_d from Table 1, Fig. 9a and Table 3, it is clear that decreased SO_4 and SO_2 emissions from the United States are responsible for the decreases of the warm water cloud droplet number concentrations from the CALIPSO retrieval, which is consistent with the satellite observations of SO_2 (Krotkov et al., 2016). In addition to the decreased SO_4 , however, the regression model based on the MODIS N_d dataset also attributes the long-term variations of N_d to the variations of black carbon. Similar correlations also exist in the eastern parts of America (region 7 in Fig. 10). The inconsistent contributions of the MODIS and CALIPSO methods represent the different retrieval methods of N_d . However, the two methods both capture the effect of the main contribution predictor (SO_4) to the long-term variations of N_d .

For the western coast of South Africa (region 11 in the Fig. 9c and d), we find that the observed $\Delta\log_{10}(N_d)$ from MODIS and CALIPSO both show consistency with the variations of $\Delta\log_{10}(\text{SO}_4)$ and $\Delta\log_{10}(\text{BC})$. These results demonstrate the important roles of BC when determining the long-term variations of N_d over the Atlantic region off of southern African (see Fig. 11b). Indeed, previous studies have shown that the aerosol emissions from the southern African biomass burning may significantly increase the droplet number concentrations (Bennartz, 2007; Wilcox et al., 2009).

To quantify the impacts of different predictors to the regional and

Table 2

The regression coefficients of different predictors in model for CALIPSO and MODIS (bold values) N_d datasets of supercooled water clouds. In addition, the correlation coefficient (R) and RMSE of the regression model in each region are also listed.

Reg.	ω	SO ₄	SO ₂	BC	OC	DUST	SS	R	RMSE
R1	0.005	0.18	0.04	0.16	0.03	-0.03	-0.01	0.46	0.23
	-	0.14	-0.01	0.19	0.02	-	-0.09	0.30	0.25
R2	0.0001	0.20	0.16	0.19	-0.11	0.06	0.07	0.62	0.21
	-	0.17	0.11	0.10	-0.08	0.09	0.001	0.44	0.22
R3	-0.02	0.12	0.13	0.24	-0.16	0.12	-	0.40	0.24
	-0.01	0.14	0.10	-	-	0.13	-	0.37	0.22
R4	-0.01	0.16	0.16	-0.13	0.26	0.04	0.07	0.61	0.25
	-0.01	0.19	0.13	-0.08	0.13	0.09	0.06	0.59	0.23
R5	-	-	0.04	-0.32	0.49	0.06	0.09	0.42	0.27
	0.003	0.08	0.03	-0.43	0.56	0.11	-	0.41	0.28
R6	-	-	-	-0.33	0.53	-	0.15	0.35	0.27
	-	-	-	-0.46	0.61	-	0.10	0.34	0.23
R7	-0.003	0.32	0.12	-0.06	0.04	0.05	0.02	0.58	0.22
	-	0.31	0.04	-0.17	0.08	0.06	0.03	0.46	0.21
R8	-0.005	0.27	0.005	-0.47	0.42	-0.02	-0.02	0.32	0.26
	-0.002	0.28	0.001	-0.45	0.33	-0.01	0.01	0.26	0.29
R9	-0.003	0.24	0.04	-0.03	0.008	0.09	-0.04	0.37	0.19
	-	0.25	0.01	-0.26	0.17	0.005	-0.06	0.25	0.19
R10	-	-	-	0.06	-	-0.11	-	0.10	0.20
	0.01	-	0.05	-	-	-	0.07	0.14	0.22
R11	0.01	-	-	0.41	-0.25	0.13	-	0.30	0.21
	-	0.07	-	0.08	-	0.13	-	0.27	0.21
R12	-0.01	0.16	-0.02	-0.01	0.07	0.04	0.04	0.30	0.24
	-	0.13	-0.02	-0.15	0.10	0.08	0.02	0.22	0.23
R13	-0.02	0.20	0.05	0.05	0.01	0.001	0.05	0.45	0.20
	-0.01	0.15	0.03	0.12	-0.05	0.02	0.04	0.34	0.19
R14	-	-	0.08	-	0.22	0.08	-	0.41	0.29
	-	-	0.05	0.18	-	0.10	-	0.37	0.27
R15	0.001	0.13	-0.02	0.27	-0.14	-0.07	0.21	0.49	0.23
	-	0.15	-0.05	0.11	0.01	-0.10	0.16	0.34	0.26
R16	-0.02	0.07	0.04	-0.14	0.06	0.12	0.06	0.35	0.16
	0.02	0.06	0.05	-0.06	0.03	0.05	0.02	0.17	0.17
R17	-0.02	0.09	0.06	-0.05	0.04	0.02	0.09	0.38	0.16
	0.01	0.10	0.06	-0.03	0.05	-0.02	0.03	0.22	0.16
R18	-	0.07	0.04	-	-	-	-	0.16	0.19
	-	-	0.07	-	-	-	-	0.15	0.21
R19	-0.004	0.15	0.04	-0.04	0.08	-0.001	0.04	0.30	0.22
	0.01	0.12	0.04	-0.03	0.06	0.02	0.03	0.24	0.22

global N_d anomalies, we further calculate the relative contributions of each variable to the regional $\Delta \log_{10}(N_d)$ based on the following equation (Huang and Yi, 1991):

$$R_j = \frac{1}{m} \sum_{i=1}^m \left[\frac{T_{ij}^2}{\sum_{j=1}^a T_{ij}^2} \right] \tag{6}$$

where m is the length of the data series, a is the number of independent variables, $T_{ij} = b_j x_{ij}$, b_j denotes the regression coefficients of each term, x_{ij} represents the predictor variables, and j is the number of predictor variables. Fig. 11 gives the detailed contribution rates of the different factors to the supercooled and warm water clouds N_d anomalies. In most regions, those aerosol types with negative regression coefficients make only small contributions to the variability of N_d and, thus, do not cause the larger uncertainties in our statistical results. Over the stratocumulus regions (region 8, 9, 11 and 12), the contribution factors are consistent between the MODIS and CALIPSO retrievals. Thus, the SO₄, SO₂ and dust over the western coast of southern American (region 9) contribute 70–80% of the variability of the warm water clouds, whereas most of the variability of the N_d over the western coast of northern Africa (region 12) is caused by the SO₄, dust and vertical velocity. Generally, the long-term variations of N_d for warm water clouds in most of regions are dominated by the variations of SO₄ and SO₂. This result agrees with the recent studies from McCoy et al. (2017b, 2017c), which demonstrate that the decadal trend in N_d is mainly driven by the sulfate mass concentration. In our results, we find that the contributions of SO₄ and SO₂ to the global averaged warm water cloud droplet number anomalies account for 60% and 55% of the CALIPSO and MODIS

retrievals, respectively. That is, the variations of SO₄ and SO₂ dominate the decreasing trends of the globally averaged N_d of warm water clouds. In addition to SO₄ and SO₂, however, the variations of OC also play an important role in determining the decreasing trends of the globally averaged N_d of supercooled water clouds. From Fig. 11, it is clear that the contributions of SO₄ and SO₂ to the supercooled water cloud droplet number anomalies are smaller than those of the warm water clouds. Meanwhile, the contributions of BC and OC increase with height, especially over the western coast of America (region 8) and southern America (region 5 and 6). Differing from the results from North America, the variations of the sulfate mass concentrations (that is, SO₄ and SO₂) over East China (region 1) caused by emission controls contribute only approximately 35% of the variability of the N_d of warm water clouds due to the sulfur dioxide over this region doesn't show monotonic variation as the east coast of North America (McCoy et al., 2017c). In summary, the contributing factors and their rates are obviously different for supercooled and warm water clouds and vary among different regions, temperatures and methods used. Of course, the present study also suffers from some uncertainties in the N_d retrieval method and the aerosol type reanalysis. In view of the main advantage of the CALIPSO retrieval being its weak dependence upon the adiabatic assumption, further studies might focus on the much wider assessment of the MERRA2 aerosol profile using the ground- or satellite-based observations (e.g., CALIPSO) (Buchard et al., 2015, 2017) in order to reduce the uncertainties of the interactions between clouds and aerosols.

Table 3
Same as Table 2, except for warm water clouds.

Reg.	ω	SO ₄	SO ₂	BC	OC	DUST	SS	R	RMSE
R1	-0.005	0.06	0.08	-0.04	0.07	0.07	0.09	0.46	0.17
	0.01	-	0.02	-	-	-	0.02	0.13	0.17
R2	-0.01	0.33	0.11	-0.08	0.005	0.03	-0.05	0.52	0.22
	-	0.31	0.04	-0.16	0.07	0.03	-	0.38	0.22
R3	-	-	0.12	0.45	-0.26	-0.04	-	0.37	0.21
	-	-	0.10	0.38	-0.27	-	-	0.27	0.21
R4	-0.02	0.21	0.08	0.11	0.07	-0.02	-0.02	0.47	0.24
	-0.01	0.15	0.09	0.05	0.09	-0.002	-0.01	0.41	0.23
R5	-0.004	-0.02	0.05	0.06	0.14	0.02	0.04	0.38	0.19
	-	-0.04	0.04	-0.05	0.23	0.06	-0.03	0.34	0.19
R6	-0.01	0.06	0.12	-	0.13	0.05	0.12	0.47	0.17
	-	0.08	0.06	-	0.10	0.04	0.05	0.35	0.16
R7	-0.001	0.16	0.07	0.11	-0.04	0.02	0.01	0.43	0.19
	0.01	0.17	0.04	-0.001	-0.02	-0.02	0.03	0.31	0.19
R8	-0.01	0.32	0.05	0.02	0.07	0.13	0.0004	0.49	0.16
	-	0.19	0.07	0.09	0.06	0.09	-0.03	0.47	0.14
R9	-0.01	0.25	0.05	0.001	0.05	0.13	0.02	0.43	0.15
	0.02	0.19	0.05	-0.03	0.05	0.09	-0.03	0.38	0.13
R10	-0.02	0.10	0.03	-	-	-0.04	0.15	0.39	0.15
	-0.005	0.17	-	-0.19	0.12	-	0.05	0.24	0.14
R11	-	0.19	-	0.09	-	0.06	0.08	0.40	0.13
	-	0.18	0.04	0.07	-	0.05	0.04	0.39	0.12
R12	-0.03	0.30	-0.02	0.09	-0.02	0.05	0.06	0.44	0.18
	0.01	0.19	0.02	0.05	-0.002	0.04	0.03	0.34	0.16
R13	-0.01	0.04	0.08	0.06	0.05	-0.002	-0.01	0.31	0.22
	0.004	0.06	0.05	0.05	0.04	0.01	-0.02	0.23	0.22
R14	-	0.13	0.08	-	-	-	-	0.29	0.22
	-	-	-	0.12	-	-	-0.08	0.14	0.24
R15	-0.01	0.19	0.06	0.06	-0.06	0.11	0.02	0.49	0.19
	0.01	0.23	-0.01	0.03	-0.06	0.05	-0.02	0.36	0.19
R16	-0.03	0.05	0.05	-0.09	0.06	0.15	-0.02	0.26	0.21
	0.03	0.04	0.04	-0.002	0.01	0.07	-0.002	0.22	0.21
R17	-0.02	0.08	0.07	-0.03	0.09	0.001	-0.0001	0.28	0.25
	0.03	0.07	0.06	-0.02	0.09	-0.03	-0.04	0.28	0.23
R18	-0.01	0.09	0.03	-0.02	0.07	0.004	0.11	0.38	0.18
	-	0.15	0.01	0.05	0.02	0.05	-0.02	0.24	0.20
R19	-0.01	0.14	0.06	0.01	0.07	0.03	0.01	0.35	0.20
	0.01	0.10	0.05	0.05	0.03	0.02	-0.03	0.28	0.19

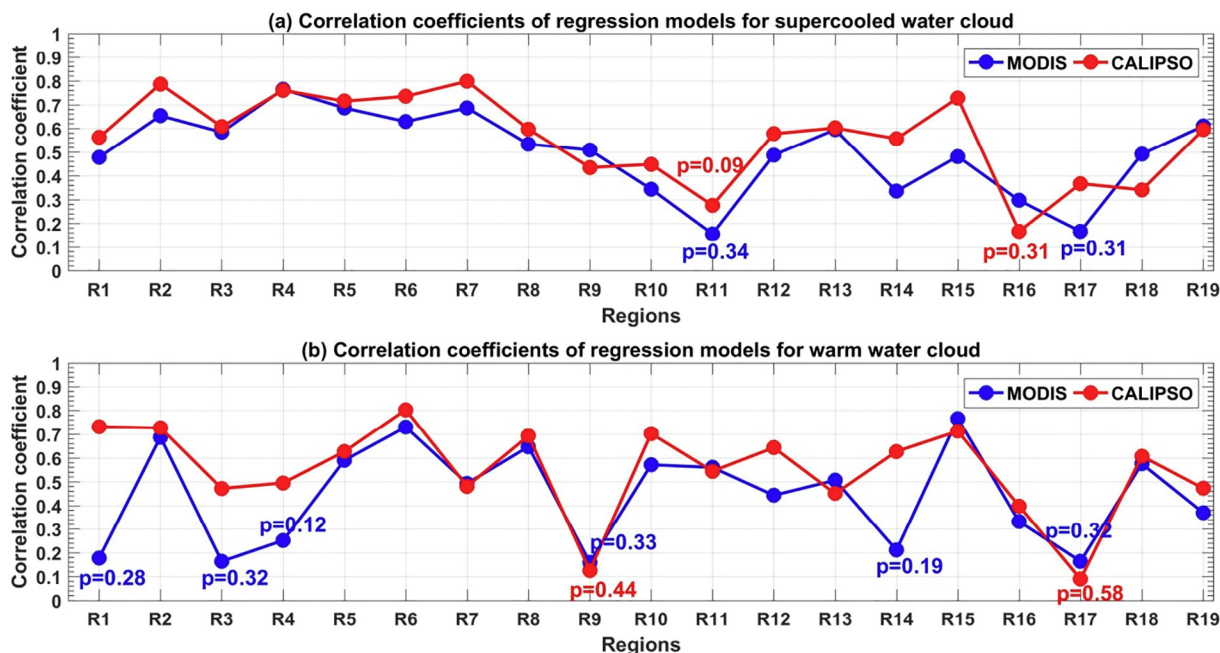


Fig. 8. The correlation coefficients between observed and predicted regional averaged $\Delta \log_{10}(N_d)$ in different regions for supercooled and warm water clouds, respectively. We also provide the confidence level (p value) if confidence level < 95%.

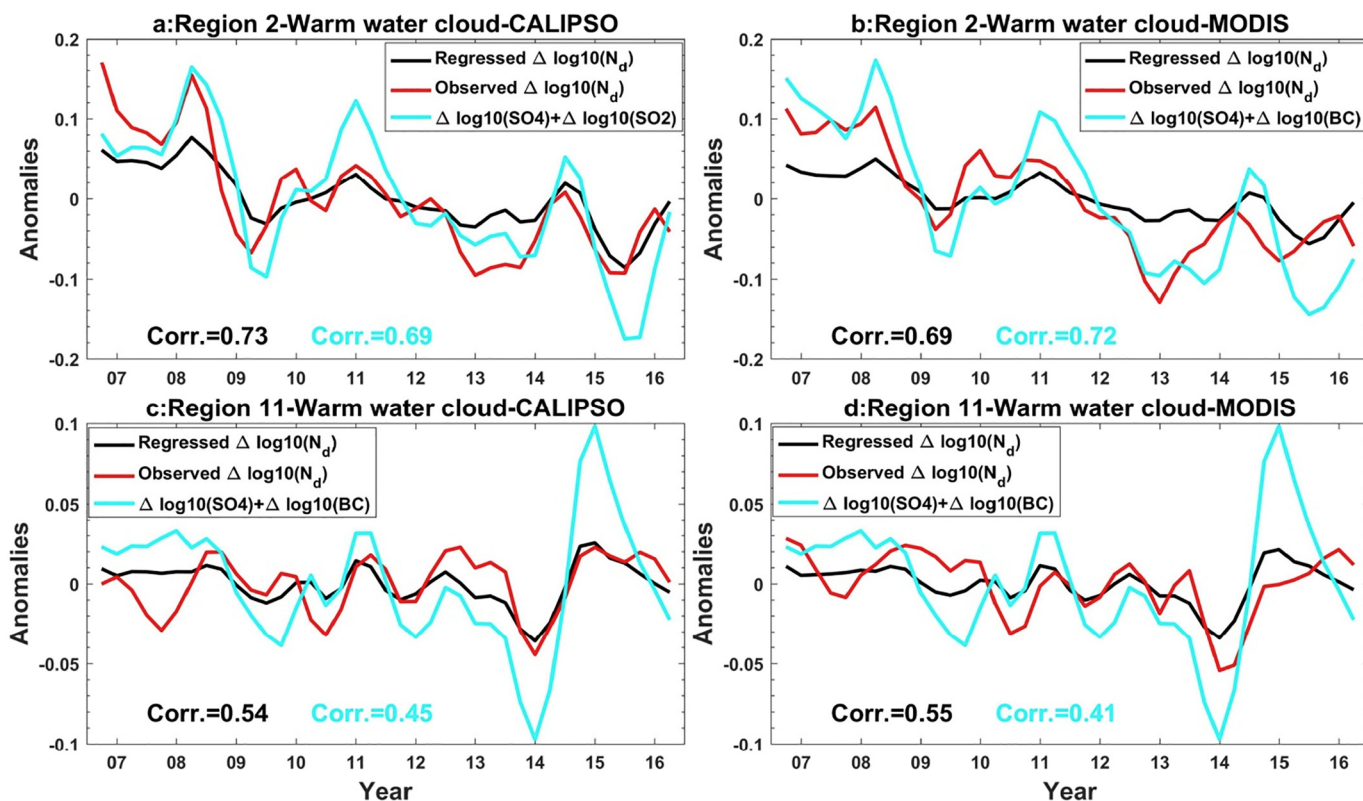


Fig. 9. The time series of regional means of regressed (black line) and observed $\Delta \log_{10}(N_d)$ (red line) in some selected regions for CALIPSO and MODIS datasets. Based on the regression coefficient, the combined time series of the two main predictors also are provided (cyan line). In addition, the correlation coefficients between regressed and observed $\Delta \log_{10}(N_d)$ (black color), and the correlation coefficients between observed $\Delta \log_{10}(N_d)$ and predictors are also listed (cyan color). (For interpretation of the references to color in this figure legend, the reader is referred to the web version of this article.)

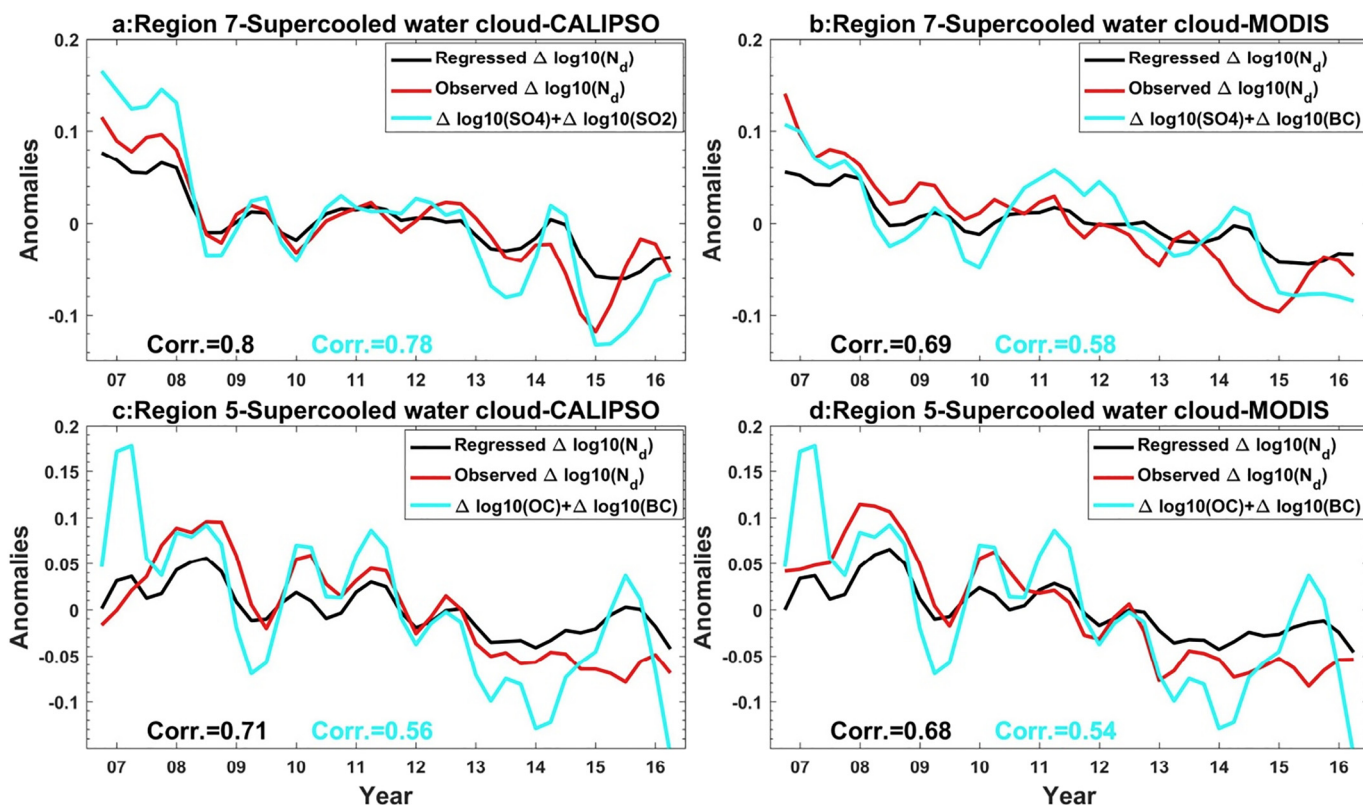


Fig. 10. Same as Fig. 9, except for regions 5 & 7 and supercooled water clouds.

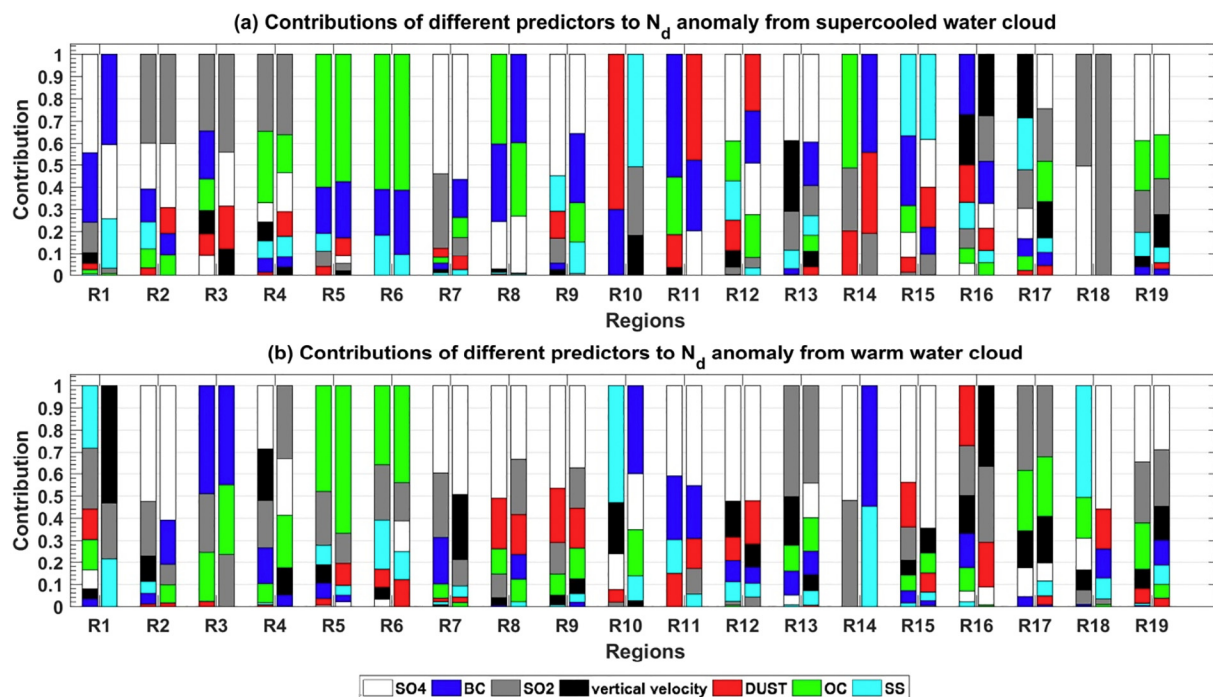


Fig. 11. The detailed contribution rates of different factors on supercooled and warm water clouds N_d anomalies. For each region, left bar is for CALIPSO and right bar corresponding the MODIS.

4. Conclusions

As one of important microphysical cloud properties, the cloud droplet number concentration (N_d) plays a key role in affecting the terrestrial radiative budget by modulating the shortwave cloud albedo (Wood, 2012). In addition, a recent study has noted that the N_d can significantly reduce the impact of the meteorological co-variations in the correlations between the global mean aerosol optical depth and cloud fraction by adding it into the above correlation (Gryspeerd et al., 2016). Thus, a refined retrieval method and the establishment of a long-term N_d dataset necessarily narrow the uncertainties of the first indirect effect of the model simulations. This study presents a new 10-year N_d dataset based on accurate depolarization ratio measurements from CALIPSO and the effective radius retrievals of clouds from MODIS (Hu et al., 2007a). Differing from the widely used passive retrieval method (e.g., MODIS retrieval), which is based on the adiabatic assumption, the retrieval method of the new N_d dataset is independent of the adiabatic assumption for the clouds and eliminates the possible bias caused by multilayer clouds. We analyze the global distribution and long-term variation of N_d by comparing the two retrieval methods. Although some statistical results agree reasonably well with those of the previous studies, new insights are also acquired.

After limiting the cloud layer number to 1, we find that the MODIS and CALIPSO retrieval methods provide very consistent global distributions of N_d , but the N_d from CALIPSO is systemically lower than that of MODIS due to the entrainment processes at the cloud tops. The comparisons of the annual cycles of N_d and the time series of the seasonal anomalies show that high consistencies between the two methods tend to occur in the stratocumulus region, which is near to the adiabatic assumption. Benefiting from the relatively accurate cloud phase discrimination of CALIPSO, this study also discusses the long-term variations of the N_d of supercooled water clouds. Generally, the N_d of supercooled water clouds are obviously smaller than those resulting from warm water clouds. In addition, the correlation between the two N_d climatologies decreases with temperature.

Model simulations indicated that the aerosol index can accurately predict the changes of N_d via a comparison with the aerosol optical

depth (Gryspeerd et al., 2017). However, it is difficult to provide a global vertical profile of the aerosol index based on only passive observations, thus limiting its utilization at different atmospheric levels. Instead of the aerosol index, our study uses the aerosol mass concentration profile from the MERRA2 aerosol reanalysis dataset to evaluate the impacts of different aerosol types on the long-term variations of N_d . Multiple regression models and contribution calculations show that the variability of the sulfate mass concentration (that is, the variability of SO_4 and SO_2) dominates the long-term variation of N_d over most regions. These results agree well with the relationship derived from recent studies (McCoy et al., 2017b, 2017c). In addition to SO_4 and SO_2 , the impacts of BC and OC on N_d also should not be ignored, especially over the important biomass burning regions.

Recently, supercooled water clouds have received widespread attention because of their significant radiative effect and poor simulations in reanalysis and climate models (Hu et al., 2010; Li et al., 2017; Matus and L'Ecuyer, 2017; Morrison et al., 2011). Our study first evaluates the effects of aerosol types and vertical velocities on the long-term variations of N_d for supercooled water clouds. The statistical results show that the contributing factors and rates for supercooled clouds are obviously different from warm water clouds. Also such contributing factors and rates vary from regions to regions, temperatures and methods used. Thus, these results emphasize the importance of the vertical variations of aerosol properties (e.g., those of composition, concentration and mixed state). The climatology described in this work provides a detailed comparison between the different methods and demonstrates that the vertically resolved ability of CALIOP may provide a useful tool for building a long-term temperature-dependent N_d dataset. However, some potential uncertainties in the retrieval methods of N_d (e.g., drizzling and horizontal heterogeneity) and aerosol reanalysis should be considered in future studies to further narrow the first indirect effects of the model simulations.

Acknowledgements

This research was jointly supported by the Foundation for Innovative Research Groups of the National Science Foundation of

- 519–536.
- Li, S., Chen, L., Fan, M., Tao, J., Wang, Z., Yu, C., Si, Y., Letu, H., Liu, Y., 2016. Evaluation of GEOS-Chem and GOCART simulated aerosol profiles using CALIPSO observations over the contiguous United States. *Aerosol Air Qual. Res.* 16, 3256–3265 (AAQR-15-03-OA-0173.R2).
- Li, J., Lv, Q., Zhang, M., Wang, T., Kawamoto, K., Chen, S., Zhang, B., 2017. Effects of atmospheric dynamics and aerosols on the fraction of supercooled water clouds. *Atmos. Chem. Phys.* 17, 1847–1863. <http://dx.doi.org/10.5194/acp-17-1847-2017>.
- Lindblom, J., Nordell, B., 2006. Water production by underground condensation of humid air. *Desalination* 189, 248–260.
- Lohmann, U., Feichter, J., 2005. Global indirect aerosol effects: a review. *Atmos. Chem. Phys.* 5, 715–737. <http://dx.doi.org/10.5194/acp-5-715-2005>.
- Lohmann, U., Feichter, J., Penner, J., Leaitch, R., 2000. Indirect effect of sulfate and carbonaceous aerosols: a mechanistic treatment. *J. Geophys. Res.* 105 (12), 193–206.
- Lohmann, U., Stier, P., Hoose, C., Ferrachat, S., Kloster, S., Roeckner, E., Zhang, J., 2007. Cloud microphysics and aerosol indirect effects in the global climate model ECHAM5-HAM. *Atmos. Chem. Phys.* 7, 3425–3446.
- Lu, M.-L., Conant, W.C., Jonsson, H.H., Varutbangkul, V., Flagan, R.C., Seinfeld, J.H., 2007. The Marine Stratus/Stratocumulus Experiment (MASE): aerosol-cloud relationships in marine stratocumulus. *J. Geophys. Res.* 112, D10209. <http://dx.doi.org/10.1029/2006JD007985>.
- Martin, G.M., Johnson, D.W., Spice, A., 1994. The measurement and parameterization of effective radius of drops in warm stratocumulus clouds. *J. Atmos. Sci.* 51, 1823–1842.
- Matus, A.V., L'Ecuyer, T.S., 2017. The role of cloud phase in Earth's radiation budget. *J. Geophys. Res.* 122, 2559–2578. <http://dx.doi.org/10.1002/2016JD026141>.
- McCoy, D.T., Burrows, S.M., Wood, R., Grosvenor, D.P., Elliott, S.M., Ma, P.-L., Rasch, P.J., Hartmann, D.L., 2015. Natural aerosols explain seasonal and spatial patterns of Southern Ocean cloud albedo. *Sci. Adv.* 1 (6).
- McCoy, D.T., Eastman, R., Hartmann, D.L., Wood, R., 2017a. The change in low cloud cover in a warmed climate inferred from AIRS, MODIS, and ERA-Interim. *J. Clim.* 30 (10), 3609–3620.
- McCoy, D.T., Bender, F.A.M., Mohrmann, J.K., Hartmann, D.L., Wood, R., Grosvenor, D.P., 2017b. The global aerosol-cloud first indirect effect estimated using MODIS, MERRA and AeroCom. *J. Geophys. Res.* <http://dx.doi.org/10.1002/2016JD026141>.
- McCoy, D.T., Bender, F.A.M., Grosvenor, D.P., Mohrmann, J.K., Hartmann, D.L., Wood, R., Field, P.R., 2017c. Predicting decadal trends in cloud droplet number concentration using reanalysis and satellite data. *Atmos. Chem. Phys. Discuss.* <http://dx.doi.org/10.5194/acp-2017-811>. (in review).
- Miles, N.J., Verlinde, J., Clothiaux, E.E., 2000. Cloud droplet size distributions in low-level stratiform clouds. *J. Atmos. Sci.* 57, 295–311.
- Minnis, P., Huang, J., Lin, B., Yi, Y., Arduim, R., Fan, T., Ayers, J.K., Mace, G.G., 2007. Ice cloud properties in ice-over-water cloud systems using Tropical Rainfall Measuring Mission (TRMM) visible and infrared scanner and TRMM microwave imager data. *J. Geophys. Res.* 112, D06206. <http://dx.doi.org/10.1029/2006JD007626>.
- Molod, A., Takacs, L., Suarez, M., Bacmeister, J., 2015. Development of the GEOS-5 atmospheric general circulation model: evolution from MERRA to MERRA2. *Geosci. Model Dev.* 8 (5), 1339–1356.
- Morrison, A.E., Siems, S.T., Manton, M.J., 2011. A three-year climatology of cloud-top phase over the Southern Ocean and North Pacific. *J. Clim.* 24 (9), 2405–2418.
- Myers, T.A., Norris, J.R., 2016. Reducing the uncertainty in subtropical cloud feedback. *Geophys. Res. Lett.* 43, 2144–2148. <http://dx.doi.org/10.1002/2015GL067416>.
- Novakov, T., Penner, J.E., 1993. Large contribution of organic aerosols to cloud-condensation-nuclei concentrations. *Nature* 365 (6449), 823.
- Nowottnick, E.P., Colarco, P.R., Welton, E.J., da Silva, A., 2015. Use of the CALIOP vertical feature mask for evaluating global aerosol models. *Atmos. Meas. Tech.* 8, 3647–3669. <http://dx.doi.org/10.5194/amt-8-3647-2015>.
- O'Dowd, C.D., Smith, M.H., Consterdine, I.E., et al., 1997. Marine aerosol, sea-salt, and the marine sulphur cycle: a short review. *Atmos. Environ.* 31 (1), 73–80.
- Painemal, D., Zuidema, P., 2011. Assessment of MODIS cloud effective radius and optical thickness retrievals over the Southeast Pacific with VOCALS-REX in situ measurements. *J. Geophys. Res.* 116, D24206. <http://dx.doi.org/10.1029/2011JD016155>.
- Platnick, S., King, M.D., Meyer, K.G., Wind, G., Amarasinghe, N., Marchant, B., Arnold, G.T., Zhang, Z.B., Hubanks, P.A., Ridgway, B., Riedi, J., 2015. MODIS cloud optical properties: user guide for the collection 6 level-2 MOD06/MYD06 product and associated level-3 datasets, version 1.0, October 2015. available at: http://modis-atmos.gsfc.nasa.gov/_docs/C6MOD06OPUserGuide.pdf (last access: 16 August 2017).
- Platnick, S., Meyer, K.G., King, M.D., Wind, G., Amarasinghe, N., Marchant, B., Arnold, G.T., Zhang, Z.B., Hubanks, P.A., Holz, R.E., Yang, P., Ridgway, W.L., Riedi, J., 2017. The MODIS cloud optical and microphysical products: collection 6 updates and examples from terra and aqua. *IEEE Trans. Geosci. Remote Sens.* 55, 502–525. <http://dx.doi.org/10.1109/tgrs.2016.2610522>.
- Quaas, J., Boucher, O., Bellouin, N., Kinne, S., 2008. Satellite-based estimate of the direct and indirect aerosol climate forcing. *J. Geophys. Res.* 113, D05204. <http://dx.doi.org/10.1029/2007JD008962>.
- Quaas, J., et al., 2009. Aerosol indirect effects-general circulation model intercomparison and evaluation with satellite data. *Atmos. Chem. Phys.* 9 (22), 8697–8717.
- Ramaswamy, V., et al., 2001. Radiative forcing of climate change. In: Houghton, J.T., et al. (Eds.), *Climate Change 2001*. Cambridge Univ. Press, New York, pp. 349–416.
- Rausch, J., Meyer, K., Bennartz, R., Platnick, S., 2017. Differences in liquid cloud droplet effective radius and number concentration estimates between MODIS collections 5.1 and 6 over global oceans. *Atmos. Meas. Tech.* 10, 2105–2116. <http://dx.doi.org/10.5194/amt-10-2105-2017>.
- Reutter, P., Su, H., Trentmann, J., Simmel, M., Rose, D., Gunthe, S.S., Wernli, H., Andreae, M.O., Pöschl, U., 2009. Aerosol- and updraft-limited regimes of cloud droplet formation: influence of particle number, size and hygroscopicity on the activation of cloud condensation nuclei (CCN). *Atmos. Chem. Phys.* 9, 7067–7080. <http://dx.doi.org/10.5194/acp-9-7067-2009>.
- Rosenfeld, D., Williams, E., Andreae, M.O., Freud, E., Pöschl, U., Rennó, N.O., 2012. The scientific basis for a satellite mission to retrieve CCN concentrations and their impacts on convective clouds. *Atmos. Meas. Tech.* 5, 2039–2055. <http://dx.doi.org/10.5194/amt-5-2039-2012>.
- Rosenfeld, D., Zheng, Y., Hashimshoni, E., et al., 2016. Satellite retrieval of cloud condensation nuclei concentrations by using clouds as CCN chambers. *Proc. Natl. Acad. Sci.* 113 (21), 5828–5834.
- Ruehl, C.R., Davies, J.F., Wilson, K.R., 2016. An interfacial mechanism for cloud droplet formation on organic aerosols. *Science* 351 (6280), 1447–1450.
- Ryan, R.T., Blau Jr., H.H., von Thüna, P.C., Cohen, M.L., Roberts, G.D., 1972. Cloud microstructure as determined by an optical cloud particle spectrometer. *J. Appl. Meteorol.* 11, 149–156.
- Schmidt, J., Wandinger, U., Malinka, A., 2013. Dual-field-of-view Raman lidar measurements for the retrieval of cloud microphysical properties. *Appl. Opt.* 52, 2235–2247.
- Schmidt, J., Ansmann, A., Bühl, J., Baars, H., Wandinger, U., Müller, D., Malinka, A.V., 2014. Dual-FOV Raman and Doppler lidar studies of aerosol-cloud interactions: simultaneous profiling of aerosols, warm-cloud properties, and vertical wind. *J. Geophys. Res.* 119, 5512–5527. <http://dx.doi.org/10.1002/2013JD020424>.
- Schmidt, J., Ansmann, A., Bühl, J., Wandinger, U., 2015. Strong aerosol-cloud interaction in altocumulus during updraft periods: lidar observations over central Europe. *Atmos. Chem. Phys.* 15, 10687–10700. <http://dx.doi.org/10.5194/acp-15-10687-2015>.
- Schuller, L., Bennartz, R., Fischer, J., Brenguier, J.L., 2005. An algorithm for the retrieval of droplet number concentration and geometrical thickness of stratiform marine boundary layer clouds applied to MODIS radiometric observations. *J. Appl. Meteorol.* 44, 28–38. <http://dx.doi.org/10.1175/JAM-2185.1>.
- Seethala, C., Horváth, Á., 2010. Global assessment of AMSR-E and MODIS cloud liquid water path retrievals in warm oceanic clouds. *J. Geophys. Res.* 115, D13202. <http://dx.doi.org/10.1029/2009JD012662>.
- Seethala, C., Norris, J.R., Myers, T.A., 2015. How has subtropical stratocumulus and associated meteorology changed since the 1980s? *J. Clim.* 28, 8396–8410.
- Shupe, M.D., Kollias, P., Persson, P.O.G., McFarquhar, G.M., 2008. Vertical motions in arctic mixed phase stratus. *J. Atmos. Sci.* 65, 1304–1322.
- Slingo, A., Brown, R., Wrench, C.L., 1982. A field study of nocturnal stratocumulus; III. High resolution radiative and microphysical observations. *Q. J. R. Meteorol. Soc.* 108, 145–165.
- Snider, J.R., Guibert, S., Brenguier, J.L., Putaud, J.P., 2003. Aerosol activation in marine stratocumulus clouds: 2. Kohler and parcel theory closure studies. *J. Geophys. Res.* 108, 8629. <http://dx.doi.org/10.1029/2002JD002692>.
- Sourdeval, O., Labonnote, L.C., Baran, A.J., Brogniez, G., 2015. A methodology for simultaneous retrieval of ice and liquid water cloud properties. Part I: information content and case study. *Q. J. R. Meteorol. Soc.* 141 (688), 870–882.
- Sourdeval, O., Labonnote, L.C., Baran, A.J., Müllmstädt, J., Brogniez, G., 2016. A methodology for simultaneous retrieval of ice and liquid water cloud properties. Part II: near-global retrievals and evaluation against A-Train products. *Q. J. R. Meteorol. Soc.* 142, 3063–3081. <http://dx.doi.org/10.1002/qj.2889>.
- Sullivan, S.C., Lee, D., Oreopoulos, L., et al., 2016. Role of updraft velocity in temporal variability of global cloud hydrometeor number. *Proc. Natl. Acad. Sci.* 113 (21), 5791–5796.
- Sun, J., Ariya, P.A., 2006. Atmospheric organic and bio-aerosols as cloud condensation nuclei (CCN): a review. *Atmos. Environ.* 40 (5), 795–820.
- Sun-Mack, S., Minnis, P., Smith, W.L., Hong, G., Chen, Y., 2017. In: Detection of single and multilayer clouds in an artificial neural network approach. *Proc. SPIE* 10424, Remote Sensing of Clouds and the Atmosphere XXII, 1042408. <http://dx.doi.org/10.1117/12.2277397>. (13 October).
- Trenberth, K.E., Fasullo, J.T., 2010. Simulation of present-day and twenty-first-century energy budgets of the southern oceans. *J. Clim.* 23, 440–454.
- Twomey, S., 1977. Influence of pollution on shortwave albedo of clouds. *J. Atmos. Sci.* 34 (7), 1149–1152.
- Wang, W., Huang, J., Minnis, P., Hu, Y., Li, J., Huang, Z., Ayers, J.K., Wang, T., 2010. Dusty cloud properties and radiative forcing over dust source and downwind regions derived from A-Train data during the Pacific Dust Experiment. *J. Geophys. Res.* 115. <http://dx.doi.org/10.1029/2010JD014109>.
- Wang, K., Yahya, K., Zhang, Y., Hogrefe, C., Pouliot, G., Knote, C., Hodzic, A., Jose, R.S., Perez, J.L., Jimenez-Guerrero, P., Baro, R., Makar, P., Bennartz, R., 2015. A multi-model assessment for the 2006 and 2010 simulations under the Air Quality Model Evaluation International Initiative (AQMEI) Phase 2 over North America: part II. Evaluation of column variable predictions using satellite data. *Atmos. Environ.* 115, 587–603. <http://dx.doi.org/10.1016/j.atmosenv.2014.07.044>.
- Wang, T., Fetzer, E.J., Wong, S., et al., 2016. Validation of MODIS cloud mask and multilayer flag using CloudSat-CALIPSO cloud profiles and a cross-reference of their cloud classifications. *J. Geophys. Res.* 121 (19), 11620–11635.
- West, R.E.L., Stier, P., Jones, A., Johnson, C.E., Mann, G.W., Bellouin, N., Partridge, D.G., Kipling, Z., 2014. The importance of vertical velocity variability for estimates of the indirect aerosol effects. *Atmos. Chem. Phys.* 14, 6369–6393. <http://dx.doi.org/10.5194/acp-14-6369-2014>.
- Wilcox, E.M., Harshvardhan, Platnick, S., 2009. Estimate of the impact of absorbing aerosol over cloud on the MODIS retrievals of cloud optical thickness and effective radius using two independent retrievals of liquid water path. *J. Geophys. Res.* 114, D05210. <http://dx.doi.org/10.1029/2008jd010589>.
- Wood, R., 2012. Stratocumulus clouds. *Mon. Weather Rev.* 140, 2373–2423. <http://dx.doi.org/10.1175/MWR-D-11-00121.1>.
- Wood, R., Leon, D., Lebsock, M., Snider, J., Clarke, A.D., 2012. Precipitation driving of droplet concentration variability in marine low clouds. *J. Geophys. Res.* 117,

- D19210. <http://dx.doi.org/10.1029/2012jd018305>.
- Zeng, S., Riedi, J., Trepte, C.R., Winker, D.M., Hu, Y.X., 2014. Study of global cloud droplet number concentration with A-Train satellites. *Atmos. Chem. Phys.* 14, 7125–7134. <http://dx.doi.org/10.5194/acp-14-7125-2014>.
- Zhang, Y., Karamchandani, P., Glotfelty, T., Streets, D.G., Grell, G., Nenes, A., Yu, F.Q., Bennartz, R., 2012. Development and initial application of the global-through urban weather research and forecasting model with chemistry (GU-WRF/Chem). *J. Geophys. Res.* 117, D20206. <http://dx.doi.org/10.1029/2012jd017966>.
- Zhang, Z., Werner, F., Cho, H.M., Wind, G., Platnick, S., Ackerman, A.S., Di Girolamo, L., Marshak, A., Meyer, K., 2016. A framework based on 2-D Taylor expansion for quantifying the impacts of subpixel reflectance variance and covariance on cloud optical thickness and effective radius retrievals based on the bispectral method. *J. Geophys. Res.* 121, 7007–7025. <http://dx.doi.org/10.1002/2016jd024837>.
- Zhao, C., Xie, S., Klein, S.A., Protat, A., Shupe, M.D., McFarlane, S.A., Comstock, J.M., Delanoë, J., Deng, M., Dunn, M., Hogan, R.J., Huang, D., Jensen, M.P., Mace, G.G., McCoy, R., O'Connor, E.J., Turner, D.D., Wang, Z., 2012. Toward understanding of differences in current cloud retrievals of ARM ground-based measurements. *J. Geophys. Res.* 117, D10206. <http://dx.doi.org/10.1029/2011JD016792>.
- Zhao, C., Qiu, Y., Dong, X., Wang, Z., Peng, Y., Li, B., Wu, Z., Wang, Y., 2018. Negative aerosol-cloud relationship from aircraft observations over Hebei, China. *Earth Space Sci.* 5. <http://dx.doi.org/10.1002/2017EA000346>.
- Zuidema, P., Westwater, E.R., Fairall, C., Hazen, D., 2005. Ship-based liquid water path estimates in marine stratocumulus. *J. Geophys. Res.* 110, D20206. <http://dx.doi.org/10.1029/2005JD005833>.